

# Photocorrosion of n- and p-Type Semiconducting Oxide-Covered Metals: Case Studies of Anodized Titanium and Copper

Håvard Wilson, Arnoul Van Rooij, Ken Jenewein, Julius Knöppel, Attila Kormányos, Serhiy Cherevko, Svein Sunde, and Andreas Erbe\*

Illumination affects corrosion of oxide-covered metals via photoinitiated dissolution processes. Herein, anodized titanium with n-type semiconducting anatase  $\text{TiO}_2$  and anodized copper with p-type semiconducting cuprite  $\text{Cu}_2\text{O}$  of thicknesses up to  $\approx 90$  nm are prepared, and investigated under controlled convection in photoelectrochemical experiments illuminated at grazing incidence. Illumination with photon energies above the bandgap triggers anodic photocurrents for titanium above the flat band potential, and cathodic photocurrents for copper below the flat band potential. Increased corrosion rates are evidenced via measurements of polarization curves, electrochemical impedance spectra (EIS) and concentration determination via inductively coupled plasma mass spectrometry (ICP-MS). The increase in corrosion current with illumination is slightly lower than photocurrents, and scales linearly with intensity as expected if triggered by linear absorption. Following the Gerischer model, for titanium, electron-hole pairs cause oxide dissolution by hole annihilation through cation dissolution. For copper, increased corrosion rates are caused by increased cathodic reaction rate through photoexcitation. The maximum nonthermal increase in corrosion rate is  $\approx 1 \mu\text{A cm}^{-2}$  for copper, and  $\approx 7 \mu\text{A cm}^{-2}$  for titanium, few micrometers per year and negligible for structural materials. Photocorrosion may affect localized corrosion, and nanostructures, for example, if morphology is crucial for a functional surface, as in catalysts.

## 1. Introduction


In many applications, structural materials are exposed to illumination. It is thus a natural question to ask if, how, and under which circumstances illumination can affect corrosion processes of metals. For oxide-covered iron and steels, different mechanisms have been attributed to cause the observed effect of light on corrosion, i) the typical upward band bending for n-type semiconducting oxides (as most spontaneously forming oxides are<sup>[1]</sup>) leading to hole migration to the oxide/solution interface and thus metal dissolution,<sup>[2,3]</sup> ii) the nontypical downward band bending where electrons migrate to the oxide–electrolyte interface and reduce  $\text{O}_2$  while holes oxidize the metal at the metal–oxide interface,<sup>[4,5]</sup> iii) induced convection through heating,<sup>[6–9]</sup> and iv) thermal effects in oxide films.<sup>[3]</sup> There is thus some controversy regarding the mechanism of how light can affect a corrosion process. From the different models referred to previously provided details, (i) and (ii) are mutually exclusive,<sup>[3]</sup> and (iii) may lead to experimental observations

which could be mistaken for (ii).<sup>[8]</sup> However, on a more general basis, seemingly contradictory results have been obtained for some systems. For example, both cathodic<sup>[10]</sup> and anodic<sup>[11,12]</sup> photocurrents have been reported for illuminated zinc. For iron and steel, both positive and negative open-circuit potential (OCP) shifts have been reported.<sup>[3,8]</sup> Analyzing only the OCP as done in some works<sup>[4,5,13]</sup> can, however, lead to misinterpretations.<sup>[3,8]</sup>

Table 1 shows an overview of relevant photocorrosion studies of metals, and the diversity of suggested mechanisms. It must be noted here that photoeffects on the dominating corrosion products do of course also affect the band structure and character of the corrosion products. Summarizing, there are a number of works in the photocorrosion literature including models with unconventional band bending for several systems.<sup>[4,5,13,14]</sup> These models are not physically impossible; they could explain results if, for example, for a metal with an n-type oxide the flat band potential is higher than the corrosion potential, but still effects of light are observed.<sup>[15]</sup> However, for strongly disordered oxides which are typical for thin oxide films in corrosion, the flat

H. Wilson, A. Van Rooij, S. Sunde, A. Erbe  
Department of Materials Science and Engineering  
NTNU, Norwegian University of Science and Technology  
7491 Trondheim, Norway  
E-mail: cuti-photocorrosion@the-passivists.org

K. Jenewein, J. Knöppel, A. Kormányos, S. Cherevko  
Forschungszentrum Jülich GmbH  
Helmholtz Institute Erlangen-Nürnberg for Renewable Energy  
Cauerstr. 1, 91058 Erlangen, Germany

 The ORCID identification number(s) for the author(s) of this article can be found under <https://doi.org/10.1002/pssa.202100852>.

© 2022 The Authors. physica status solidi (a) applications and materials science published by Wiley-VCH GmbH. This is an open access article under the terms of the Creative Commons Attribution License, which permits use, distribution and reproduction in any medium, provided the original work is properly cited.

DOI: 10.1002/pssa.202100852

**Table 1.** Overview over photocorrosion studies; studies without strong mechanistic discussion element and studies pre-1990 have not been included. Cond.—conditions, Irrad.—irradiation.

Metal	Cond.	Irrad.	Effect of illumination	Explanation	Ref.
Carbon steel	Natural sea water	Sunlight	Slightly increased current consumption during cathodic protection; increased corrosion rate	Heating of steel surface, induced convection and thus increased oxygen transport	[7,6]
Carbon steel	3.5% NaCl	UV	Corrosion rate 9× higher when illuminated	Increased conductivity of oxide through illumination; hole migration to oxide/solution interface	[67]
Carbon/weathering steel	NaCl-ind. atm. corr.	UV	Increased corrosion rate	Photogenerated holes migrate to n-type oxide/Fe interface and oxidize Fe; effect on dominant corrosion products and transformations between those; holes facilitate chloride adsorption	[81,4,15,5,82]
Carbon steel	Running water	UV	Increased mass loss	Photogenerated holes migrate to solution/oxide interface, dissolve oxide	[2]
Carbon steel	NaCl soln. + cysteine	VIS	Increased inhibitor efficiency	Photogenerated holes migrate to oxide/metal interface, oxidize metal; decreased interfacial electron transfer	[83]
Iron	Buffered Cl <sup>-</sup>	325 nm	Inhibition of pit nucleation	Photoquenching of electric field; modification of the vacancy/electronic structure	[84,85]
Stainless steel	NaCl sol., different pH	UV	Inhibition of pitting corrosion	Photoquenching of electric field in passive film	[86–88]
Stainless steel	NaCl sol., different pH	UV	Higher pitting potential, extended initiation time, also when illuminating before electrochemical experiments; differences with pH	Illumination affects the composition of the passive layer; photoinactive outer layer formed at higher pH	[89]
Stainless steel	0.1 M H <sub>2</sub> SO <sub>4</sub>	UV	Increased stability of passive film, decreased passive current	Illumination affects the composition and electronic structure of the passive layer	[90]
Stainless steel	NaCl; acidic Cl <sup>-</sup>	UV	Higher light intensity accelerated pitting	Photoactivation of MnS inclusions; reduced stability of passive films	[91,92]
Brass	NaCl-ind. atm. corr.	UV	Increased corrosion rate	Photogenerated holes migrate to oxide/metal interface, oxidize metal	[93]
Bronze	Cl <sup>-</sup> , SO <sub>4</sub> <sup>2-</sup> , HCO <sub>3</sub> <sup>-</sup>	UV/VIS	Increased (VIS) and decreased (UV) corrosion rates	Electron-hole pair formation and transfer in different oxides	[94]
Copper	Waste water	UV	Increased corrosion rate	Upward band bending, migration of holes to oxide/electrolyte interface	[2]
Copper	Atm. corr. + NaCl	UV	Increased oxide formation rate	n-type cuprite formation enhanced by illumination	[95]
Copper	Borate + NaCl	VIS	Increased pitting resistance short term; increased oxide dissolution long term	Photoquenching of electric field in oxide layer; holes migrate to p-type oxide/solution interface	[14]
Copper	NaCl-ind. atm. corr.	UV	Increased corrosion rate	photogenerated holes migrate to oxide/metal interface	[57]
Copper	atm. corr. + NaCl	UV	Increased corrosion rate	Change in dominating corrosion product	[56]
Cu-alloys	Borate-buffered NaCl	UV	Increased pitting resistance	Photo-induced modification of passive film	[79]
Nickel	Waste water	UV	No effect	–	[2]
Titanium	Running water	UV	No change in corrosion rate	–	[2]
Titanium	H <sub>2</sub> SO <sub>4</sub>	UV	Increased oxide dissolution	hole accumulation at n-type oxide/electrolyte interface; weakened Ti–O bonds	[96,74,97,98]
Titanium	H <sub>2</sub> SO <sub>4</sub> + Br <sup>-</sup>	UV	Decreased pitting potential	Hole accumulation at n-type oxide/electrolyte interface; weakened Ti–O bonds	[97,98]
Titanium	Brine	UV	Increased oxide growth, no effect on pitting potential	Different layer structure during illumination	[99,100]
Titanium	atm. corr. + chloride	UV	Increased oxide growth	Photolytic H <sub>2</sub> SO <sub>4</sub> formation in solution	[101]
Silver	atm. corr., NaCl, ozone	UV	Increased corrosion rate	Generation of oxygen radicals from ozone	[102–104]
Zinc	NaCl-ind. atm. corr.	UV	Increased corrosion rate	photogenerated holes migrate to n-type oxide/Zn interface and oxidize Zn	[13]

**Table 1.** Continued.

Metal	Cond.	Irrad.	Effect of illumination	Explanation	Ref.
Zinc	Nat. aerated NaCl	488/515 nm	Increased $E_{\text{corr}}$ , anodic current	Excitation via intragap states?	[105–107]
Zinc	pH 13	Xe arc lamp	Anodic photocurrent, increased dissolution	Hole migration to n-oxide/electrolyte interface	[11,12]
Zn-based metallic coatings	Stream water/tap water	UV	Increased mass loss	Other corrosion products than n-ZnO, electron-hole pairs migrate to oxide surface and increase cathodic reaction rate	[10]

band potential is typically not very well defined and thus difficult to determine directly from Mott–Schottky analysis.<sup>[3,16]</sup> This difficulty thus contributes to the difficulties of building up consistent band diagrams for corroding metals with semiconducting oxides.

One issue which is especially severe in applications is the frequently poorly defined or even changing Fermi level of the electrolyte. In addition to the often poor control of convection in many photocorrosion studies which was already pointed out,<sup>[8]</sup> the frequently nonideal control of illumination also contributes to the difficulties of consistently analyzing photocorrosion. In almost all experimental studies, illumination is conducted at normal incidence, an illumination geometry which hinders efficient light absorption in the first nanometers at the metal/oxide interface.<sup>[17]</sup> To that end, our group developed a cell with illumination at grazing incidence, 70° angle of incidence, that enables efficient light absorption for the thin oxide films, which are important especially in the initial stages of corrosion processes<sup>[3]</sup>; this cell was also used for photoelectrochemical experiments in this work.

In photoelectrochemical energy conversion, the problem of photocorrosion of, for example, anodes in photoelectrochemical water splitting is even more critical than in structural materials.<sup>[18,19]</sup> Cu<sub>2</sub>O as one system discussed in this work is of interest for use in composite photocatalysts,<sup>[20,21]</sup> and photocathodes.<sup>[22]</sup> In contrast, photocorrosion is an issue with this system.<sup>[23]</sup> Other relevant materials for which photocorrosion data has recently become available are tungsten oxide-based photoanodes,<sup>[24]</sup> and zinc oxide single crystals.<sup>[25]</sup> Overall, special surface modification methods are used for inhibition.<sup>[26,27]</sup>

The phenomena investigated in this work can have some relevance for the mechanisms exploited in photocathodic protection. One photocathodic protection method is to connect the material in need of protection to a panel of photoanodes to produce current through semiconductor photoelectrochemistry,<sup>[28,29]</sup> for example, using TiO<sub>2</sub>.<sup>[30,31]</sup> A combination with energy storage, for example, via photocharging and discharging of WO<sub>3</sub>,<sup>[32]</sup> or via electrochemical double layer capacitors,<sup>[33]</sup> is a more recent approach to overcome the limitations of photocathodic protection to periods with illumination.<sup>[29]</sup>

Goal of this work is to conduct a systematic study of the semiconductor aspects of photocorrosion comparing a metal with an n-type oxide and a metal with a p-type oxide. Titanium and copper were studied here; TiO<sub>2</sub> is a prototypical n-type oxide, whereas Cu<sub>2</sub>O is one of the few p-type oxides that forms spontaneously on metals.<sup>[1]</sup> However, Cu<sub>2</sub>O formed in the presence of chloride,<sup>[34,35]</sup> very thin films in chloride-free NaOH,<sup>[36]</sup> or electrodeposited films<sup>[37]</sup> may also become n-type.

Experimentally, anodizing was used to grow oxides anatase TiO<sub>2</sub> and cuprite Cu<sub>2</sub>O with different thickness based on literature procedures (see Supporting Information).<sup>[38]</sup> These oxides were characterized to verify their identity and their semiconductor nature. Polarization curves and electrochemical impedance spectra (EIS) were measured in 0.5 M H<sub>2</sub>SO<sub>4</sub> for titanium, and in borate buffer at pH 9 for copper. The choice of the different electrolytes is based on different oxide solubilities and other practicalities. Dissolution measurements were conducted both ex situ and in situ<sup>[39,40]</sup> by concentration determination through ICP-MS. Electrode potentials in this work are referenced against Ag/AgCl/3 M KCl, unless noted otherwise. Full experimental details, including details on repeats are described in Section 1, Supporting Information. Uncertainty estimates are presented as standard deviation in the last digits given in brackets. Raw data for this work is available via NTNU's institutional repository.<sup>[41]</sup>

As in previous work,<sup>[3]</sup> we will discuss a net photocorrosion current density as difference between the corrosion current densities  $i_{\text{corr}}^{(\text{light})}$  in the presence and  $i_{\text{corr}}^{(\text{dark})}$  in the absence of illumination

$$\Delta i_{\text{corr}}^{(\text{photo})} = i_{\text{corr}}^{(\text{light})} - i_{\text{corr}}^{(\text{dark})} \quad (1)$$

which in general depends on the wavelength and intensity of illumination. This quantity is compared to detected photocurrent densities  $i_{\text{photo}}$ . In this work, thus, photocorrosion is considered as “loss of metal,” which is different from the consideration as “dissolution of a solid compound.” The latter view is frequently used in photo(electro)chemical energy conversion.

## 2. Results

**Figure 1** shows photocurrent and photovoltage measurements for copper and titanium samples with different oxide thicknesses. The respective initial dark currents and potentials were subtracted. Anodic current increased when illuminating titanium, while the cathodic current increased for copper (Figure 1a). The absolute current increased with increasing oxide thickness for both materials. The OCP shifted to more negative values when titanium was illuminated, while the opposite was found for copper (Figure 1b).

Typical EIS results for copper are shown in **Figure 2**. When two semicircles were observed in the complex plane diagrams, the measurements were fitted to the circuit diagram in Figure 2e, which is commonly used to analyze oxide-covered metals.<sup>[42,43]</sup> The reasoning behind the selected equivalent circuit is also illustrated in Figure 2e. In addition to the Randles circuit,

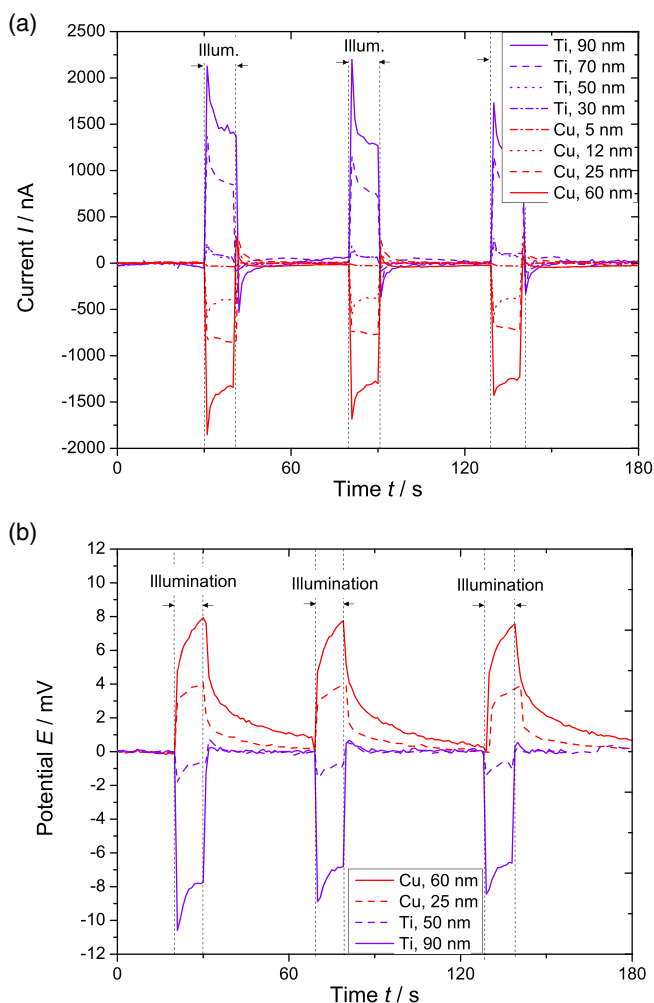


**Figure 1.** a) Photocurrent and b) photovoltage for anodized titanium in 0.5 M  $\text{H}_2\text{SO}_4$  illuminated with 320 nm monochromatic light, and anodized copper in borate buffer (pH = 9) illuminated with white light. Titanium with native oxide is not included because no response was found. Initial dark current and average potential have been subtracted.

another RQ circuit was added to account for the added capacitance of the space charge layer and the resistance of the current through the oxide. The additional elements were added in series to the Randles circuit because the space charge layer is in series with the double layer. In the case of copper, two semicircles were found for all oxide thicknesses. A general decrease in the diameter of the larger semicircle, found at lower frequencies, was observed under illumination with white light. No significant differences were found for the smaller semicircles at higher frequencies for the dark and illuminated samples. Parameters obtained from the EIS fitting are compiled in Table 2.

EIS measurements for titanium (Figure 2) show the beginning of a single semicircle; therefore, this data was fitted to a simplified equivalent circuit, where  $R_{sc}$  and  $Q_{sc}$  were excluded. Previously, this model has been used for  $\text{TiO}_2$  films<sup>[44]</sup> and hematite electrodes,<sup>[45,46]</sup> however, the physical equivalent to the electrical circuit elements differs between the two. A general

decrease in charge-transfer resistance is found when illuminating the samples with 320 nm monochromatic light.

Figure 3 shows polarization curves for titanium and copper in 0.5 M  $\text{H}_2\text{SO}_4$  and borate buffer, respectively. Monochromatic light with wavelength of 320 nm was used for illuminating the titanium samples, while white light was used for the copper samples. For titanium, a general increase in anodic current was found, while for copper, a general increase in cathodic current was found. Corrosion current densities  $i_{corr}$ , corrosion potentials  $E_{corr}$ , and the Tafel slopes obtained from the polarization curves are summarized in Table 2. An unexpected difference in the shape of polarization curves was observed for the different copper oxide thicknesses. The cause of the observed difference is not known; however, the XRD measurements (see Section 2.2, Supporting Information) showed some differences in the structure for the different copper oxide films, which could explain the different shapes of the polarization curves.

Photocurrents were measured while scanning the wavelength of the illuminating monochromatic light from 800 to 300 nm (Figure 4a). When the wavelength became sufficiently short, a photocurrent was observed. The photocurrent onset was observed around 600 nm ( $\approx 2.1$  eV) for copper and around 390 nm ( $\approx 3.2$  eV) for titanium.

Polarization curves both in the dark, and with monochromatic illumination of different wavelengths, are shown in Figure 7, Supporting Information. The polarization curves only show an effect of illumination for photon energies above the bandgap of the respective oxides. For titanium, an increase in anodic current was found, and the current increased with higher photon energies. For wavelengths 600 and 800 nm, no difference from dark conditions was found. Copper oxides exhibited a less noticeable difference between dark and illuminated conditions, but an increase in cathodic current was observed when the photon energies were above the bandgap of the copper oxides.

A comparison of  $\Delta i_{corr}^{(photo)}$  and  $i_{photo}$  is shown in Figure 4b,c.

By placing a series of different neutral density filters between the light source and the entrance of the electrochemical flow cell, different light intensities were obtained. Figure 8, Supporting Information, shows polarization curves for titanium and copper illuminated with different light intensity. Figure 5 shows  $\Delta i_{corr}^{(photo)}$  and  $i_{photo}$  as a function of transmittance. Both quantities scale linearly with intensity, however with significant uncertainty; there was an increase of anodic current for titanium and of cathodic current for copper.

Mott-Schottky plots were measured in the dark and with illumination for both copper and titanium (Figure 9, Supporting Information). The flat band potentials estimated from those plots (Table 2) are summarized in Figure 6. Copper samples showed a negative slope with flat bands between 25 and 100 mV, depending on the oxide thickness. Titanium samples showed a positive slope, with the flat band potential varying from  $-300$  to  $+250$  mV versus Ag/AgCl/3 M KCl. The measurements shown here were done at 100 Hz, however, measurements with frequencies ranging between 10 kHz and 1 Hz were performed. The flat band potential was independent of frequency between 1 Hz to 1 kHz, but the measured capacitance changed, preventing a more detailed analysis.

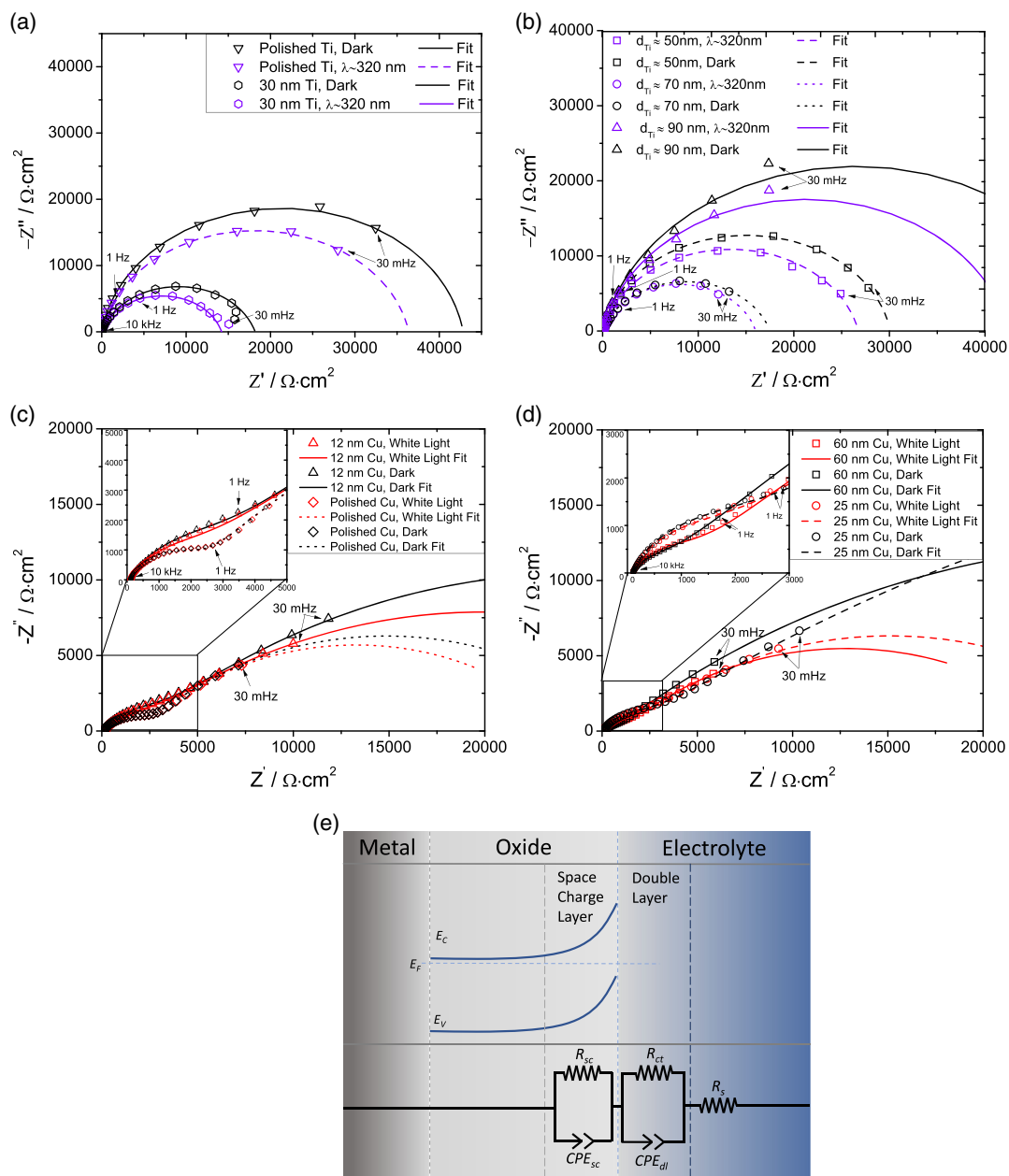


**Figure 2.** Electrochemical impedance spectra (EIS) measurements of polished and anodized a,b) titanium in 0.5 M  $\text{H}_2\text{SO}_4$  and c,d) copper in borate buffer at pH = 9; a) titanium with native oxide, 30 and 50 nm thick oxide, b) with 70 and 90 nm thick oxide; c) copper with native oxide and 12 nm thick oxide, d) with 25 and 60 nm thick oxide. e) Fitting parameters to equivalent circuit in (e) are compiled in Table 2. Elements:  $R_{sc}$ —resistance through the oxide;  $CPE_{sc}$  (parameters  $Q_{sc}$  and  $n_{sc}$ )—constant phase element of the space charge layer;  $R_{ct}$ —charge-transfer resistance;  $CPE_{dl}$  (parameters  $Q_{dl}$  and  $n_{dl}$ )—constant phase element of the double layer;  $R_s$ —solution resistance.

The potential dependence was further investigated by polarizing titanium and copper samples to potentials above and below the flat band potential. Photocurrent and EIS were measured at the different potentials (Figure 7 and 8). EIS fitting results are compiled in Table 3. No steady-state current was observed for titanium below the flat band potential, but an anodic photocurrent was measurable above the flat band potential.  $i_{photo}$  increased with potential. The transient shape also changed with potential. Close to the flat band potential, the

anodic current peaked and then decreased with time until it reached a steady state. When illumination was turned off, a cathodic current was measured immediately before the current returned to zero. However, at more positive potentials, the decrease in current disappeared and no cathodic current was measurable after illumination was shut off. The EIS measurements were independent of illumination below the flat band potential, whereas  $R_{ct}$  was reduced by illumination at potentials above the flat band.

**Table 2.** Electrochemical parameters for anodized titanium with oxide of different thickness  $d$  in 0.5 M H<sub>2</sub>SO<sub>4</sub>, and for anodized and polished copper in borate buffer (pH 9). Oxide thickness  $d$  for polished samples given here as 5 nm. Illumination: UV—320 nm monochromatic light; W—white light; D—dark. Fit results from electrochemical impedance spectra (EIS) to equivalent circuit in Figure 1. From polarization curves (Figure 3): corrosion current density  $i_{\text{corr}}$ , corrosion potential  $E_{\text{corr}}$  (versus Ag/AgCl/3 M KCl) and apparent estimated cathodic and anodic Tafel slopes,  $b_c$  and  $b_a$ , respectively. Flat band potential  $E_{\text{fb}}$  (versus Ag/AgCl/3 M KCl) and slope for the linear region of the Mott–Schottky plot (Slope MS) obtained from Mott–Schottky plots in Figure 9, Supporting Information.

	$d$ [nm]	Ill.	$R_s$ [ $\Omega$ cm <sup>2</sup> ]	$R_{\text{sc}}$ [k $\Omega$ cm <sup>2</sup> ]	$Q_{\text{sc}}$ [F <sup>1/<math>n_{\text{sc}}</math></sup> cm <sup>-2</sup> ]	$n_{\text{sc}}$	$R_{\text{ct}}$ [k $\Omega$ cm <sup>2</sup> ]	$Q_{\text{dl}}$ [F <sup>1/<math>n_{\text{dl}}</math></sup> cm <sup>-2</sup> ]	$n_{\text{dl}}$	$i_{\text{corr}}$ [ $\mu$ A cm <sup>-2</sup> ]	$E_{\text{corr}}$ [mV]	$b_c$ [mV dec. <sup>-1</sup> ]	$b_a$ [mV dec. <sup>-1</sup> ]	$E_{\text{fb}}$ [mV]	Slope MS [10 <sup>7</sup> C <sup>-2</sup> V <sup>-1</sup> ]	
Ti	5	UV	2.56(1)	NA	NA	NA	34(4)	5.6(4)E-5	0.94(1)	1.6(2)	116(8)	-415(2)	243(10)	-275(1)	0.30(2)	
		D	2.57(1)	NA	NA	NA	42(1)	6.6(2)E-5	0.92(2)	1.3(1)	131(4)	-397(4)	265(1)	-248(35)	0.5(2)	
	30	UV	2.75(3)	NA	NA	NA	15(1)	3.0(1)E-5	0.89(1)	3.57(3)	143(4)	-326(4)	490(38)	-18(46)	3.4(3)	
		D	2.72	NA	NA	NA	18	2.9E-5	0.86	3.44(2)	131(18)	-295(57)	360(17)	-27(65)	3.0(2)	
	50	UV	3.56(8)	NA	NA	NA	27(1)	3.8(1)E-5	0.89(1)	1.9(0)	115(1)	-272(21)	370(37)	-5(5)	3.9(6)	
		D	3.48	NA	NA	NA	30	3.60E-5	0.90	1.5(2)	115(11)	-226(75)	287(62)	-5(5)	4(1)	
	70	UV	2.03(1)	0.3(3)	2.8(2)E-4	0.70(2)	15.5(2)	8.9(4)E-5	0.84(4)	2.6(2)	148(6)	-183(8)	317(13)	-19(2)	2.5(3)	
		D	2.13(9)	0.03(4)	1.2(5)E-4	0.9(2)	18(1)	8.3(9)E-5	0.85(7)	2.1(3)	160(9)	-172(22)	294(27)	1(10)	4(1)	
	90	UV	3.75(1)	0.025(1)	8.6(2)E-4	1.11(1)	41.8(5)	1.1(1)E-4	0.88(1)	2.4	136	-320	599	233(6)	1.7(4)	
		D	3.71(6)	0.022(2)	7.7(6)E-4	1.13(2)	51(7)	1.1(2)E-5	0.88(1)	2.0(1)	137(21)	-297(31)	593(7)	225(9)	2(2)	
	Cu	5	W	101(2)	2.5(1)	2.5(1)E-5	0.72(1)	17(1)	3.2(1)E-4	0.65(2)	4.7(3)	-124(8)	-250(14)	153(42)	18(1)	-50(10)
			D	101(1)	2.5(1)	2.5(3)E-5	0.72(1)	19(1)	3.3(1)E-4	0.66(2)	2.6(4)	-55(5)	-396(96)	112(3)	19(2)	-50(10)
12.5		W	106(1)	2.7(5)	5.2(2)E-5	0.67(4)	25(2)	1.94(6)E-4	0.62(3)	4.2(4)	-68(12)	-253(18)	151(8)	74(2)	-23(1)	
		D	104(2)	3.0(4)	4(1)E-5	0.67(1)	37(5)	1.5(4)E-4	0.59(2)	2.4(5)	-62(12)	-309(39)	136(26)	71(1)	-21(1)	
25		W	104(2)	2.0(1)	4(2)E-5	0.77(5)	28(3)	1.8(3)E-4	0.57(4)	8.0(6)	-105(4)	-231(14)	NA	42(10)	-24(4)	
		D	96(11)	2.9(4)	5(1)E-5	0.71(4)	38(1)	2.5(5)E-4	0.60(1)	2.1(8)	-71(37)	-264(36)	114(19)	25(2)	-48(3)	
60		W	92(6)	0.786(3)	6.0(4)E-5	0.71(1)	24.2(7)	3.2(2)E-4	0.56(2)	3.5(5)	-9.2(5)	-222(7)	122(26)	82(2)	-97(4)	
		D	94(3)	0.56(1)	5.5(5)E-5	0.78(5)	44(5)	2.8(3)E-4	0.53(2)	2.7(2)	-20(3)	-317(76)	142(9)	78(8)	-120(8)	

For copper, no photocurrents were observed at potentials positive to the flat band potentials, which is opposite of what was observed for titanium. At potentials negative of the flat band potential, a cathodic photocurrent was measurable. However, the transient shape did not change, as opposed to the behavior for titanium. No significant effect was observed at potentials above the flat band potential, though the average values of many of the EIS fitting parameters differed between the illuminated and dark samples, the results were overlapping within the relatively large standard deviations. For potentials below the flat band potential, however, significant differences between illuminated and dark EIS measurements were observed, both  $R_{\text{ct}}$  and  $R_{\text{sc}}$  decreased with illumination. Especially large effects of illumination were found at -200 mV, which corresponds to the potential with the highest capacitance measured in the Mott–Schottky plots.

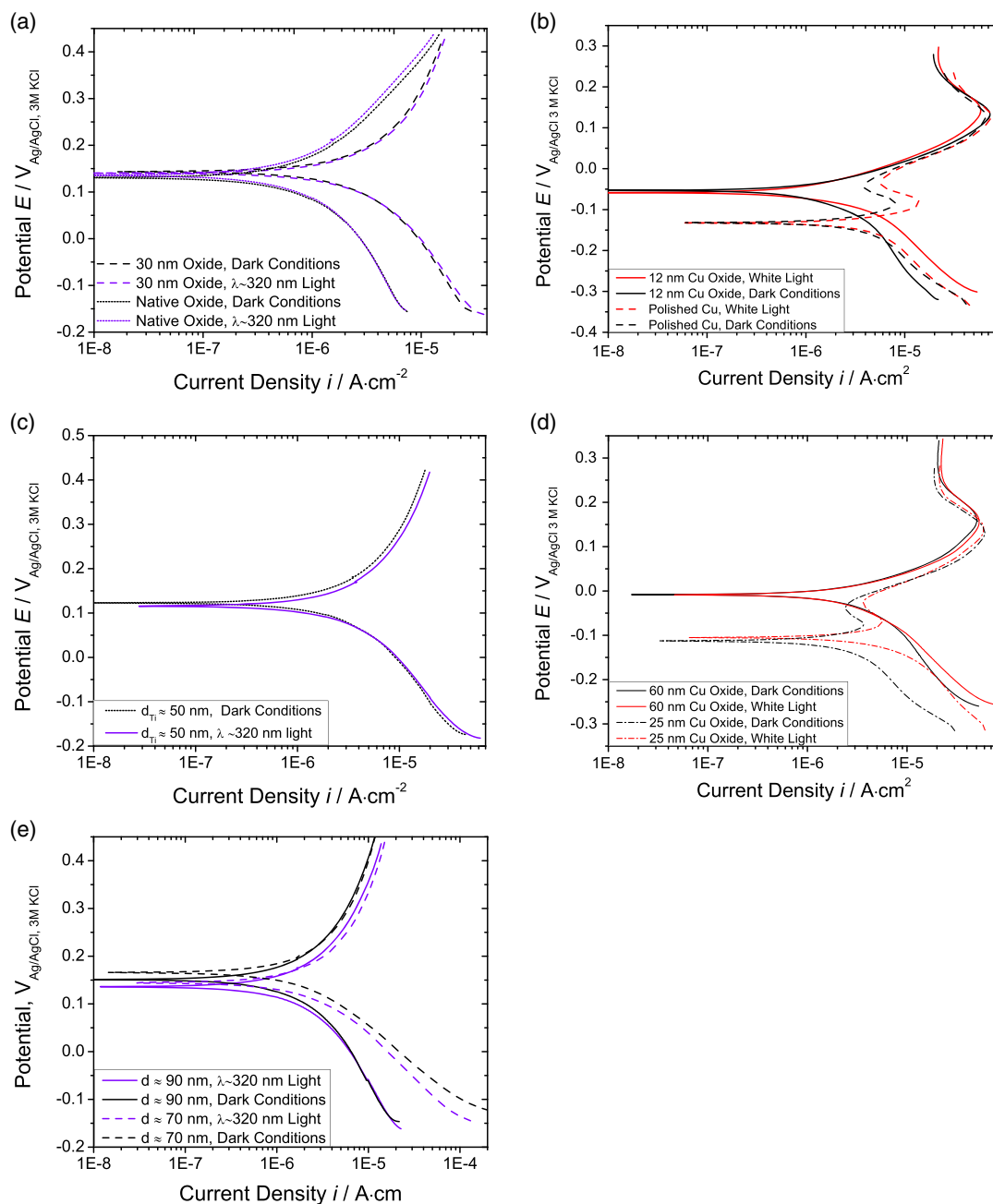
Table 4 shows results from ex situ ICP-MS analysis of electrolyte exposed to anodized titanium or copper for 7.5 h with or without illumination. For both samples, the dissolution rate was larger when illuminated at all sample times. The samples were visually inspected after exposure, and no change in the titanium's appearances was found, while the green-gold color of the copper oxide had changed to a dark brown for both the illuminated and dark sample (Figure 10, Supporting Information).

Figure 9 shows a selected result of in situ ICP-MS measurements. Titanium dissolution was found which steadily decreased with time. When illuminating the sample, the dissolution rate

increased for a short period, and after a while started to decrease again after illumination was shut off. Overall, thus, an increase in titanium concentration was found when illuminating at potentials above the flat band potential. Additional measurements are shown in Section 4.2, Supporting Information.

The effect of oxygen on photocorrosion was studied with galvanostatically anodized titanium, which had been characterized first. First, polarization curves of galvanostatic titanium oxide films were recorded at different illumination conditions (Figure 10a). Corrosion current density, corrosion potential, and Tafel slope values are compiled in Table 5. There was a 40-fold increase in  $i_{\text{corr}}$  for the samples illuminated with 320 nm monochromatic light compared to the dark. The average corrosion potential for both the illuminated samples were lower than in the dark; however, the white light illumination was within the uncertainty. The average difference in corrosion potential between 320 nm illumination and in dark was 154 mV. The cathodic Tafel slopes differed significantly.

The shape of the transients in photocurrent measurements at the OCP did not differ significantly from the photocurrent transients for potentiostatically anodized titanium. The steady-state photocurrent for these specific films was 0.20(2)  $\mu$ A cm<sup>-2</sup>. White light illumination resulted in a steady-state photocorrosion current of 0.03(1)  $\mu$ A cm<sup>-2</sup>, which is only a fraction of the steady-state photocurrent observed for 320 nm monochromatic illumination.



**Figure 3.** a,c,e) Polarization curves for titanium in 0.5 M  $\text{H}_2\text{SO}_4$  and b,d) copper in borate buffer at  $\text{pH}=9$ . Oxide thickness is indicated in the respective panel.

The effect of oxygen on the photocorrosion process was investigated for galvanostatically anodized titanium by either purging the electrolyte with nitrogen or saturating the electrolyte with oxygen. For copper, the electrolyte was either left naturally aerated, or purged with nitrogen for 20 min.

Figure 10 shows polarization curves and EIS for titanium and copper. Corrosion current density, corrosion potential, Tafel slopes, and parameters from EIS fitting for titanium and copper are compiled in Table 6.

For titanium, polarization curves were almost overlapping at potentials negative of  $E_{\text{corr}}$ , however, at potentials positive of  $E_{\text{corr}}$ , the anodic current increased significantly for the illuminated samples in both electrolytes. For the  $\text{O}_2$ -saturated electrolyte, there was an increase in the anodic current by an order of magnitude for the illuminated samples compared to the dark.

For copper, an increase in cathodic current was found when illuminating the samples. The relative increase of

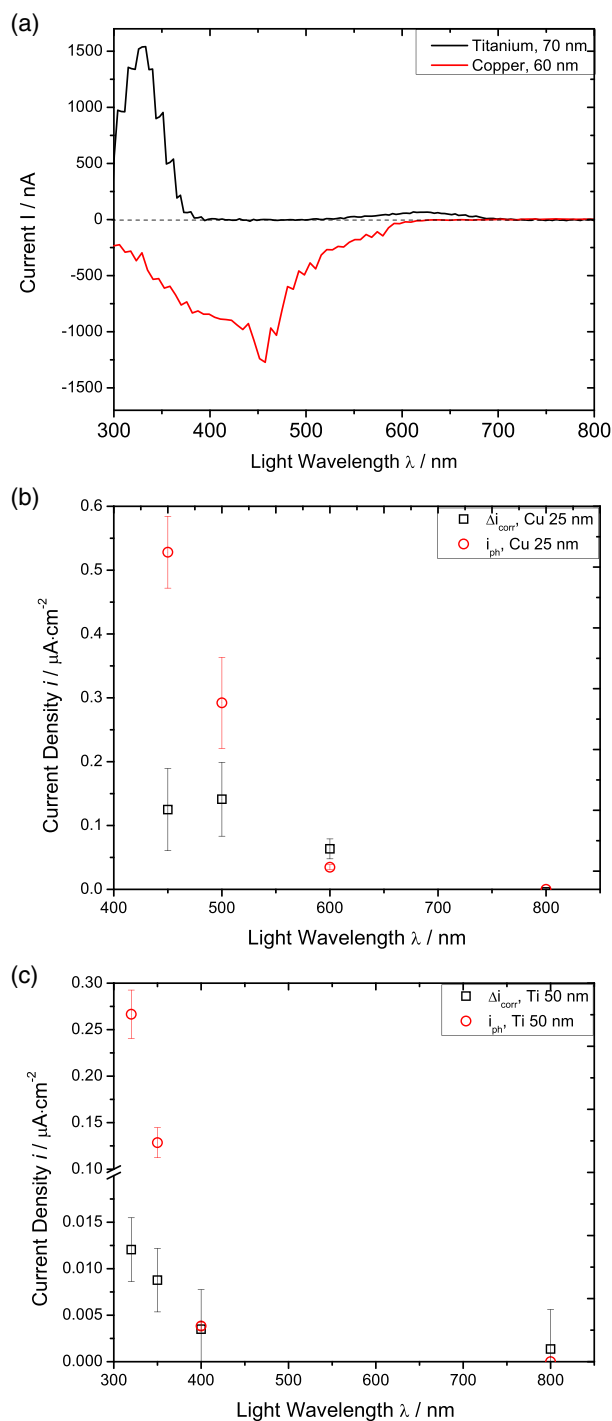


**Figure 4.** a) Photocurrent as a function of light wavelength for anodized titanium and copper in 0.5 M  $\text{H}_2\text{SO}_4$  and borate buffer (pH = 9), respectively. Current was not normalized with respect to light intensity. b)  $\Delta i_{\text{corr}}^{(\text{photo})}$  compared to  $i_{\text{ph}}^{(\text{photo})}$  of anodized copper (25 nm oxide); respective polarization curves in Figure 7a,b, Supporting Information. c)  $\Delta i_{\text{corr}}^{(\text{photo})}$  for anodized titanium (50 nm oxide) compared to  $i_{\text{ph}}^{(\text{photo})}$ ; respective polarization curves in Figure 7c, Supporting Information.

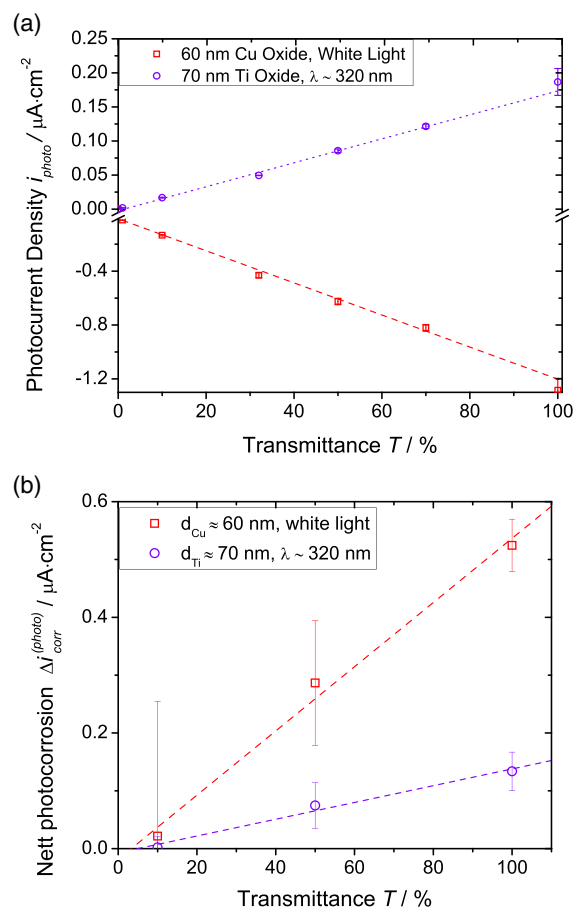


**Figure 5.** The relation between  $i_{\text{photo}}$ ,  $\Delta i_{\text{corr}}^{(\text{photo})}$ , and light intensity varied with neutral density filters of different transmittance  $T$ ;  $T = 100\%$  shows the results without any filters. Respective polarization curves in Figure 8, Supporting Information. a) Photocurrent for different intensities for anodized copper (borate buffer, pH = 9) and titanium (0.5 M  $\text{H}_2\text{SO}_4$ ). Dotted lines show the linear regression. b) Net photocorrosion current density as function of intensity. Dashed lines show linear fit.

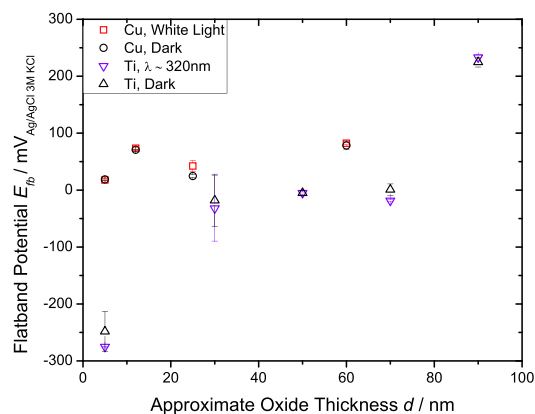


**Figure 6.** Flat band potentials for oxides with different thickness, estimated from the Mott–Schottky plots in Figure 9, Supporting Information.



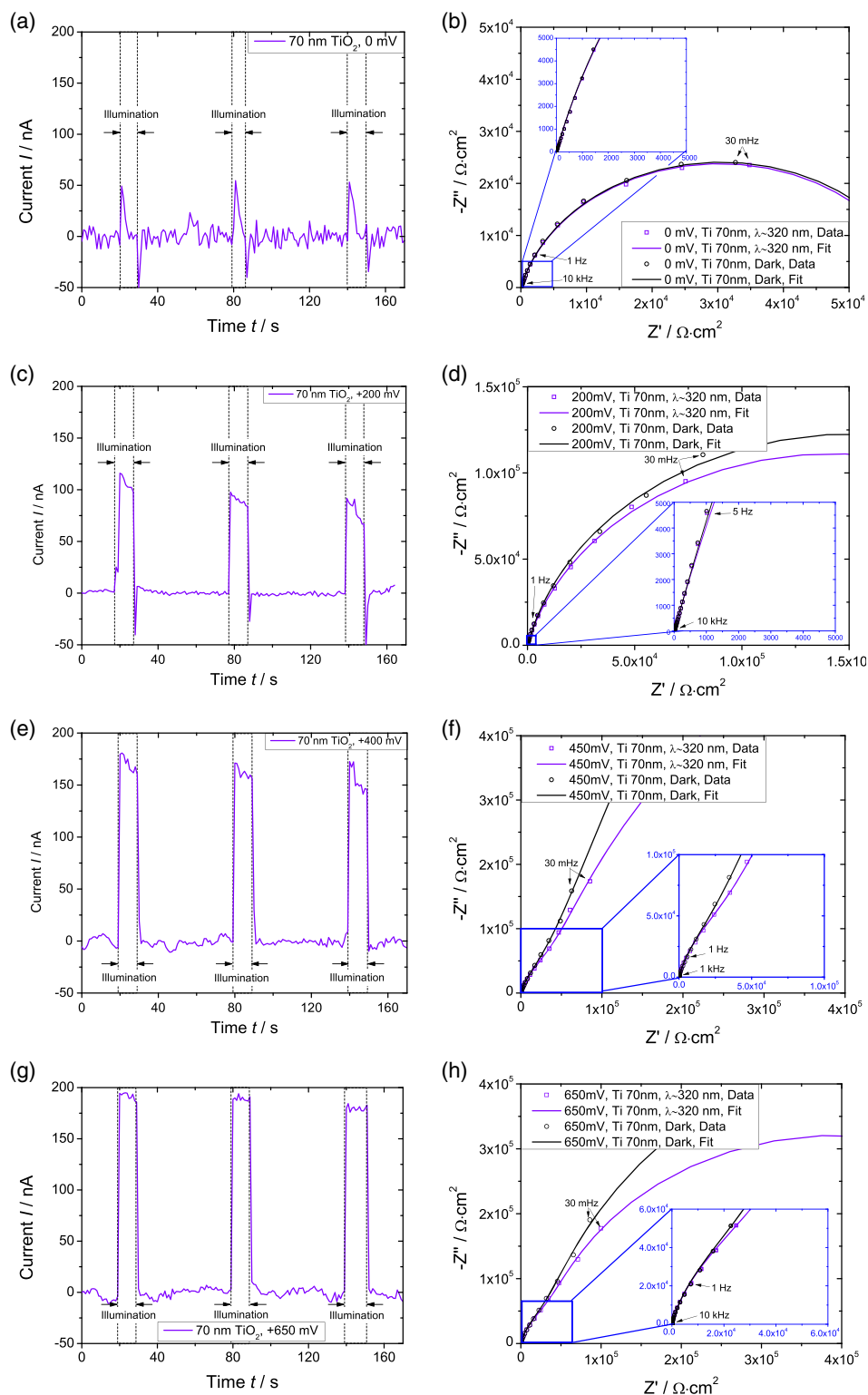


**Figure 7.** Photocurrents and EIS measured for 70 nm thick titanium oxide in 0.5 M  $\text{H}_2\text{SO}_4$  polarized to different potentials. a,c,e,g) Photocurrents at 0, 200, 450, and 650 mV, respectively; b,d,f,h) EIS at the respective potential.

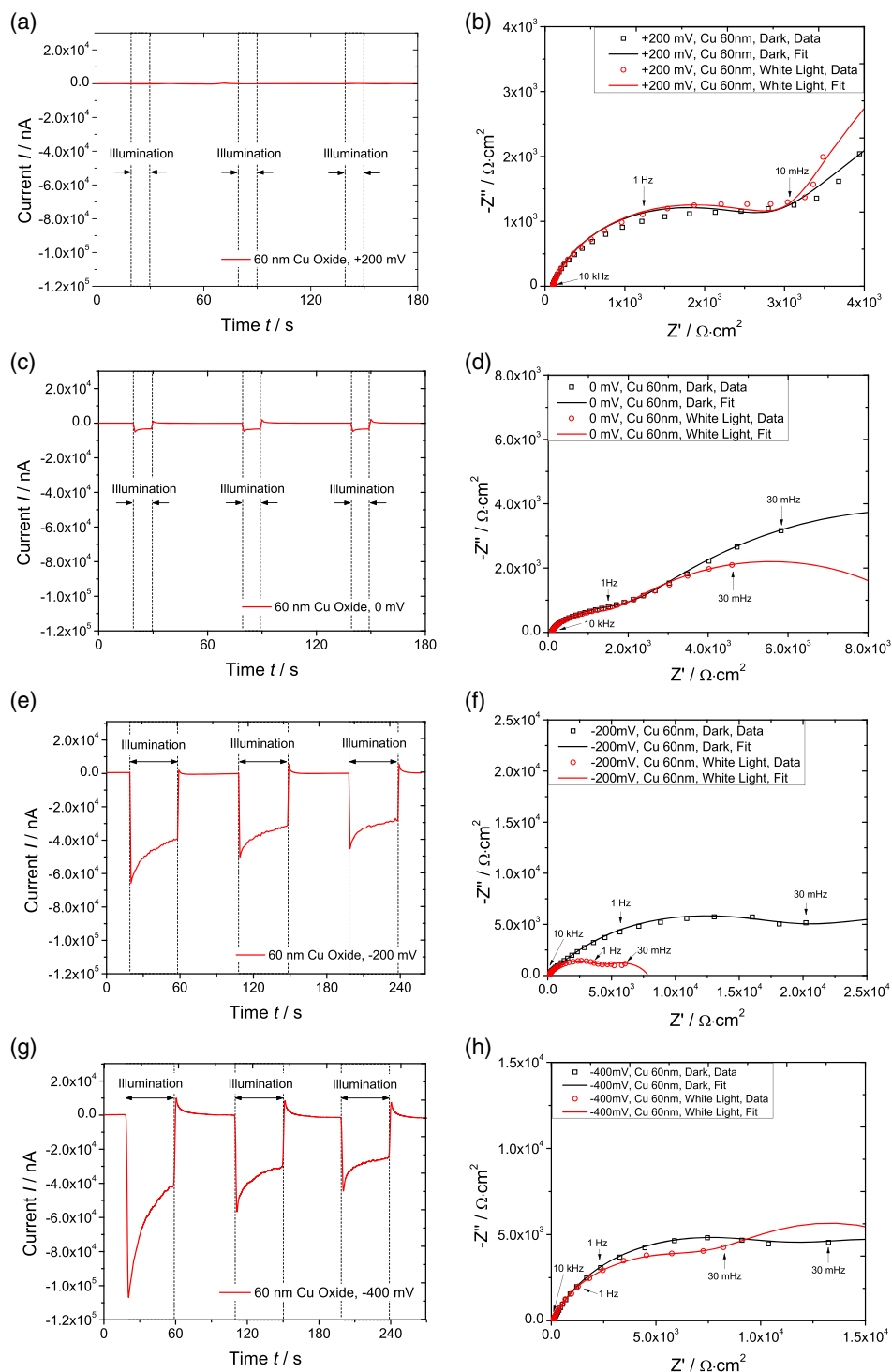


**Figure 8.** Photocurrent and EIS measurements of 60 nm copper oxide in borate buffer (pH = 9), polarized to different potentials. a,c,e,g) Photocurrents at 200, 0, -200, and -400 mV, respectively; b,d,f,h) EIS at respective potential.

cathodic current was larger for the  $N_2$ -purged electrolyte than in the aerated.

In situ reflectance spectroscopy was used to study structural changes in the oxides more closely. Results are only presented

for copper; for titanium, the resulting spectra were too noisy to permit an interpretation. Measurements for copper and the corresponding Tauc plots of  $t=150$  min are shown in **Figure 11**. For copper an increase in absorbance occurred at

**Table 3.** Fitting parameters of EIS experiments in Figure 7 for 70 nm TiO<sub>2</sub> in 0.5 M H<sub>2</sub>SO<sub>4</sub> with and without 320 nm monochromatic illumination (top), and in Figure 8 for 60 nm copper oxide in borate buffer (pH = 9) with and without white light illumination (bottom) at different potentials. Illumination: UV—320 nm monochromatic, W—white, D—dark. Model: Figure 1.

Metal	Pot. [mV]	Ill.	$R_s$ [ $\Omega \text{cm}^2$ ]	$R_{sc}$ [ $\Omega \text{cm}^2$ ]	$Q_{sc}$ [ $\text{F}^{1/n_{sc}} \text{cm}^{-2}$ ]	$n_{sc}$	$R_{ct}$ [ $\Omega \text{cm}^2$ ]	$Q_{dl}$ [ $\text{F}^{1/n_{dl}} \text{cm}^{-2}$ ]	$n_{dl}$
Ti	650	UV	2.97(1)	6.0(2)E + 4	1.75(4)E-5	0.856(3)	5.4(5)E + 5	3.10(4)E-5	1.045(3)
		D	2.98(2)	5.8(8)E + 4	1.8(1)E-5	0.85(1)	6.9(4)E + 5	2.9(2)E-5	1.03(2)
	450	UV	2.97(1)	5.1(6)E + 4	2.1(3)E-5	0.84(1)	5.5(4)E + 5	3.4(3)E-5	1.04(1)
		D	2.95(2)	4.7(3)E + 4	2.5(1)E-5	0.83(1)	7(1)E + 5	3.4(1)E-5	1.02(1)
	200	UV	2.9(2)	0.3(3)	1.3(3)E-5	1.00(1)	3.0(2)E + 5	2.7(3)E-5	0.82(4)
		D	3.1(1)	1(1)	3(1)E-5	0.97(9)	3.23(2)E + 5	2.6(3)E-5	0.83(5)
0	UV	3.07(1)	2(2)	3(1)E-4	0.97(9)	5.8(4)E + 4	6.31(5)E-5	0.86(2)	
	D	2.96(7)	1(1)	3.9(8)E-4	0.99(7)	5.4(4)E + 4	6.29(6)E-5	0.88(1)	
Cu	200	W	90(8)	3.2(1)E + 3	8.7(9)E-5	0.80(1)	20(10)E + 3	1.8(2)E-3	0.85(5)
		D	95(1)	3.1(4)E + 3	8.1(6)E-5	0.82(1)	18(4)E + 3	1.2(2)E-3	0.70(7)
	0	W	83(1)	1.3(1)E + 3	6(2)E-5	0.70(2)	8.2(4)E + 3	5(1)E-4	0.56(5)
		D	87(6)	2.4(5)E + 3	2.6(4)E-5	0.64(3)	16(1)E + 3	2.2(1)E-4	0.60(2)
	-200	W	90(1)	1(2)E + 3	8(2)E-6	0.9(2)	5(1)E + 3	2(1)E-4	0.69(2)
		D	87(3)	30(8)E + 3	1.8(6)E-5	0.7(1)	26(6)E + 3	7(7)E-4	0.72(9)
	-400	W	95(2)	8.5(5)E + 3	1.34(1)E-5	0.77(4)	9.0(1)E + 3	1.2(1)E-4	0.88(1)
		D	94(2)	12(2)E + 3	7.6(7)E-5	0.78(1)	11.5(7)E + 3	1.1(1)E-3	0.74(1)

**Table 4.** Ex situ inductively coupled plasma mass spectrometry (ICP-MS) analysis of electrolyte exposed to anodized titanium (in H<sub>2</sub>SO<sub>4</sub>) and copper (in borate buffer) for an illumination time  $t_{\text{illum}}$  up to 7.5 h. Dissolution current density  $i_{\text{diss}}$  calculated from the metal concentration  $c_{\text{met}}$ . Illumination: 320 nm monochromatic (Ti) or white (Cu).

		$t_{\text{illum}}$ [min]	$c_{\text{met}}$ [ $\text{ng mL}^{-1}$ ]		$i_{\text{diss}}$ [ $\mu\text{A cm}^{-2}$ ]	
			Dark	Light	Dark	Light
Ti	H <sub>2</sub> SO <sub>4</sub> blank	0	0	–	0	–
		150	7.5(3)	21.0(1)	2.6(1)	7.2(1)
		d_oxide $\approx$ 50 nm	300	5.6(0)	10.9(2)	1.9(0)
		450	2.1(2)	4.5(2)	0.7(1)	1.5(1)
Cu	Borate buffer blank	0	0.04(1)	–	0.5(1)	–
		150	0.02(1)	0.16(1)	0.3(1)	1.6(1)
		d_oxide $\approx$ 60 nm	300	0.13(1)	0.77(2)	1.2(1)
		450	0.20(1)	1.90(8)	2.1(1)	23(1)

similar rates for both the illuminated and dark sample; however, the shape of the absorbance spectra differs. The absorbance increased from below 800 nm for the sample kept in the dark, while it increased below 700 nm for the illuminated sample. The different shape of the absorbance spectra is made even more clear in the Tauc plots. Bandgaps of 2.0 eV were found for the illuminated sample and of  $\approx$ 1.5 eV for the non-illuminated sample, following the standard analysis. Thus, there is evidence for enhanced oxide growth on copper when illuminated.

### 3. Discussion

#### 3.1. The Role of Electron-Hole Pair Formation

The results presented here show that electron-hole pairs generated in oxides can increase corrosion rates for metals with both n-type and p-type oxides. Both the titanium and copper oxides created in this work have semiconducting properties. UV-vis spectra showed absorption related to a bandgap. Monochromatic photocurrent measurement showed  $|i_{\text{photo}}| > 0$  for light with photon energies higher than the bandgap. As expected, titanium and copper had directly opposite photocurrent and photovoltage, because n- and p-type semiconductors have different minority carriers, which are responsible for the measured photocurrent. The Mott-Schottky plots indicated p-type semiconductor behavior for copper and n-type for titanium.

Electron-hole pairs contribute to dissolution of anodized titanium. The increase in titanium concentration in the electrolyte after illumination found by ICP-MS measurements, the linear relationship between light intensity and  $\Delta i_{\text{corr}}^{(\text{photo})}$  and  $i_{\text{photo}}$ , which is expected for a linear absorption process, the shape of the polarization curves, and that  $\Delta i_{\text{corr}}^{(\text{photo})}$  was highest for the thicker oxide (50–90 nm) all indicate that the holes contribute to dissolution. The fact that  $\Delta i_{\text{corr}}^{(\text{photo})}$  is highest for the thicker oxides (50–90 nm) also indicates that increased  $i_{\text{photo}}$  was related to higher corrosion current density. For titanium,  $i_{\text{photo}}$  (0.4–0.8  $\mu\text{A cm}^{-2}$  for the 50–90 nm oxides) is similar to  $\Delta i_{\text{corr}}^{(\text{photo})}$  (0.4 to 0.5  $\mu\text{A cm}^{-2}$ ). The estimated  $\Delta i_{\text{corr}}^{(\text{photo})}$  from dissolution measurements by ex situ ICP-MS gave a rate of 0.7  $\mu\text{A cm}^{-2}$ , which was in the same order of magnitude as

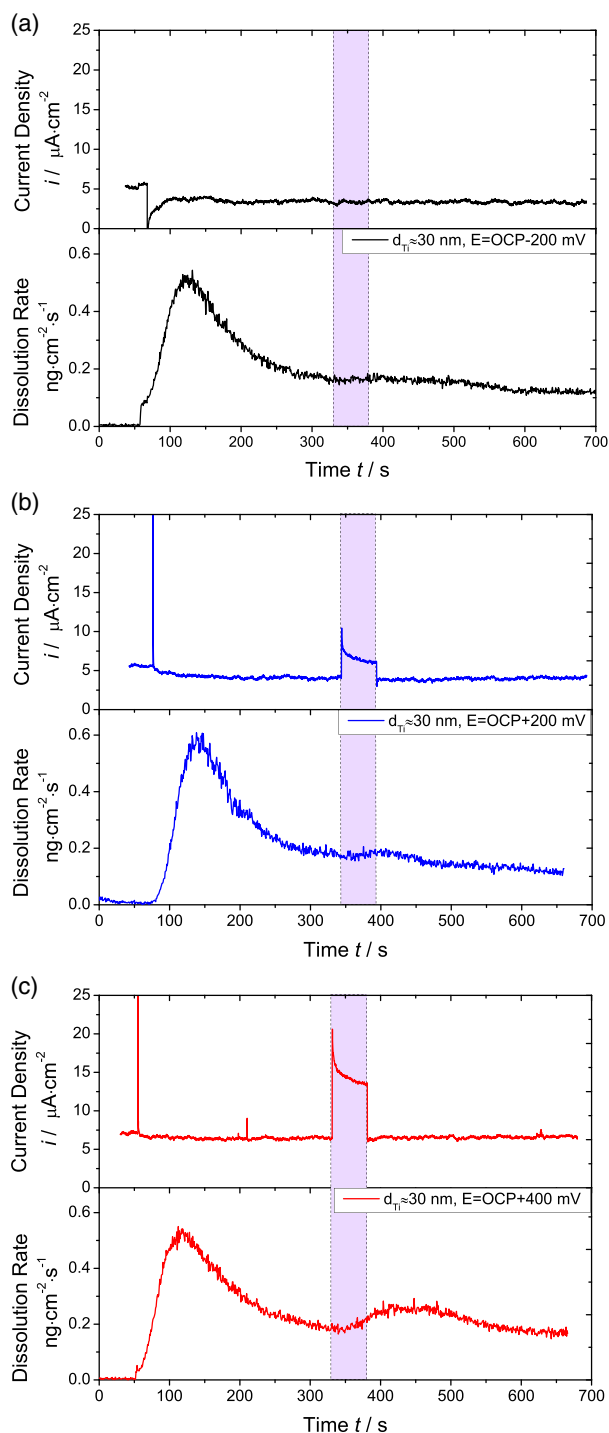
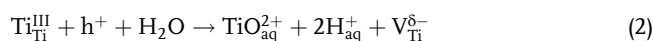


**Figure 9.** In situ inductively coupled plasma mass spectrometry (ICP-MS) measurements for 30 nm thick titanium oxide in 0.1 M H<sub>2</sub>SO<sub>4</sub>, illuminated with 385 nm monochromatic light. a) polarized to -200 mV versus open-circuit potential (OCP), b) polarized to +200 mV versus OCP, and c) polarized to +400 mV versus OCP. OCP was 125 mV versus Ag/AgCl/3 M KCl.

the electrochemical measurements. For titanium, the polarization curves showed an increase in anodic current when

illuminated. Additionally,  $\Delta i_{\text{corr}}^{(\text{photo})} > 0$ , yet the Tafel slopes were not significantly changed. The constant Tafel slopes indicate that illumination does not fundamentally change the underlying dark reactions. The EIS results showed for all oxide thicknesses that  $R_{\text{ct}}$  was reduced when illuminated, also indicating that illumination accelerated the corrosion process.

It is challenging to assign a unique dissolution scheme for titanium oxide here. Titanium is predominantly in the Ti<sup>IV</sup> state in the oxide, thus the ejection of interstitial titanium atoms after hole activation, or the shrinkage of the lattice by exclusion of a titanium vacancy are possible pathways of photodissolution. As some evidence exists also for the presence of Ti<sup>III</sup> species in the oxides under certain conditions,<sup>[47,48]</sup> a mechanism in which a hole h<sup>+</sup> reacts with a lower valent Ti atom under formation of the soluble titanyl cation TiO<sub>aq</sub><sup>2+</sup> may be thought of, schematically



where the forming vacancy has a charge  $\delta$  that compensates the excess charges in the solid oxide. This reaction is directly analogous to what has been proposed for iron by Wilson et al.<sup>[3]</sup> At high temperatures, vacancy condensation was directly observed in transmission electron microscopy,<sup>[48]</sup> which may also play a role under the conditions in this work. Thermodynamic defect levels for the different dominating defects in anatase TiO<sub>2</sub> are available in the literature,<sup>[49,50]</sup> and more recent literature also discussed the differences obtained in previous calculations.<sup>[50]</sup> As dissolution occurs from the surface, special surface or subsurface defects as suggested from density functional theory calculations<sup>[51]</sup> may be crucial in the predominant dissolution channels. Electric fields also affect the stability of the dominating defects,<sup>[52]</sup> and are inevitably present at the solid/solution interface. In aqueous solution, hydrogen in defects plays an additional role,<sup>[53]</sup> and could also be involved in the dissolution reaction.

The results also show that  $\Delta i_{\text{corr}}^{(\text{photo})} > 0$  is possible for metals covered by both n- and p-type oxides. The observed  $\Delta i_{\text{corr}}^{(\text{photo})}$ , the decreased  $R_{\text{ct}}$  with illumination, and the ICP-MS measurements showing increased dissolution when illuminated all indicate that light increases the corrosion rate of oxide-covered copper. However, the results for copper in the work do not indicate a dissolution process through hole annihilation. Holes are unlikely to dissolve the copper oxide because they are not expected to migrate toward the oxide–electrolyte interface. Instead, they can directly oxidize metallic copper at the metal–oxide interface.



Thus, oxide would grow by formation of Cu<sup>+</sup> at the metal–oxide interface, whereas hydroxide is supplied as reaction product of the cathodic reaction at the oxide–solution interface. Indeed, a thickness increase was observed, supporting this interpretation. At the metal–electrolyte interface, the dissolution reaction must involve an oxidation, which could, for example, proceed via a localized reaction with oxygen to a soluble Cu<sup>2+</sup> species.<sup>[54,55]</sup>

Mott–Schottky analysis for copper indicates p-type behavior, and the positive photovoltage and cathodic photocurrent measurements indicate that electrons migrated toward the

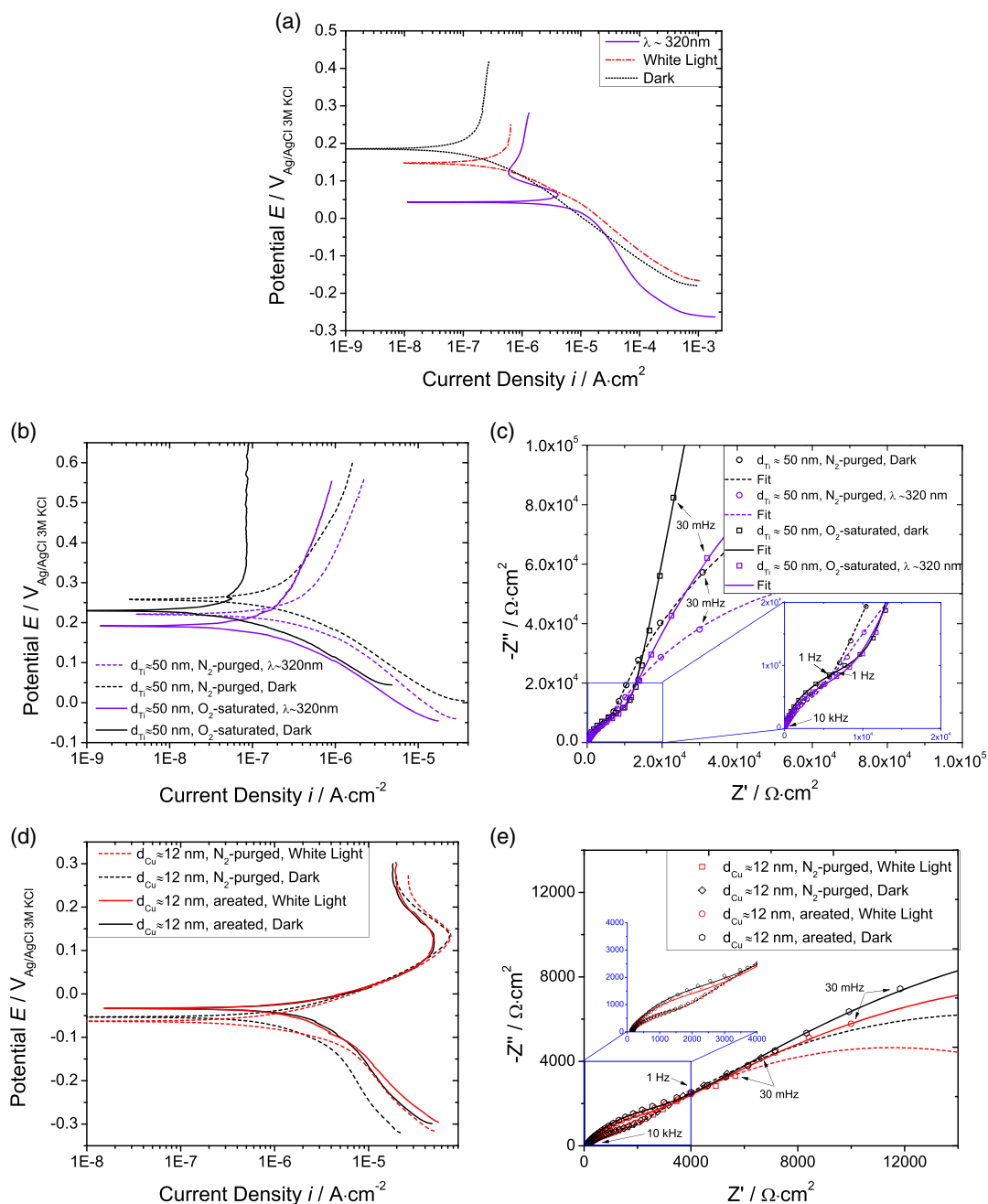


**Figure 10.** a) Polarization curves in 0.5 M  $H_2SO_4$  of galvanostatically anodized titanium with a 50 nm thick oxide. Samples were either illuminated with white light, 320 nm monochromatic light, or kept in the dark. b–d) Effect of oxygen. The 50 nm titanium oxide (galvanostatic), b) polarization curves and c) EIS, both in  $H_2SO_4$ ; 12 nm thick copper oxide d) polarization curves and e) EIS, both in borate buffer (pH = 9). Lines in EIS are fit from model in Figure 2e.

oxide–electrolyte interface. Therefore, a process where electrons contribute to accelerated cathodic reaction and thereby accelerate the corrosion rate is proposed. Some studies postulated that n-type  $Cu_2O$  must be formed to explain the increase in photocorrosion, because only anodic photocurrent should contribute to photocorrosion.<sup>[56,57]</sup> Photocorrosion of semiconductors was often studied for pure semiconductor crystals, where corrosion is mostly associated with n-type semiconductors and the hole

accumulations at the semiconductor surface. These holes then cause dissolution of the semiconductor.<sup>[58]</sup> For single-crystal p-type semiconductors, the cathodic current can be increased by excited electrons migrating to the semiconductor–electrolyte interface. Such a migration does not necessarily cause dissolution. It is therefore expected that metals covered with p-type semiconductors should not experience photocorrosion. However, applying semiconductor electrochemistry in this

**Table 5.** Corrosion current density, corrosion potential, and Tafel slopes in 0.5 M H<sub>2</sub>SO<sub>4</sub> from galvanostatically anodized titanium. Illumination: UV—320 nm monochromatic, W—white, D—dark.

Illum.	$i_{\text{corr}}$ [ $\mu\text{A cm}^{-2}$ ]	$E_{\text{corr}}$ [mV]	$b_c$ [mV dec. <sup>-1</sup> ]	$b_a$ [mV dec. <sup>-1</sup> ]
UV	7(2)	36(7)	-256(13)	NA
W	0.4(3)	168(18)	-132(4)	NA
D	0.16(5)	190(21)	-122(7)	NA

manner may not be suitable for the oxide-covered metals in this work. A passive current related to the growth or dissolution of the passive film is still present, as  $i_{\text{corr}}^{(\text{dark})} > 0$ . Applying equilibrium, semiconductor theory might not always be suitable, due to the ionic movement in the passive films.<sup>[59]</sup> Indeed, results obtained here indicate that defects generated by illumination increase ion mobility in the semiconductor films. The increase in corrosion rate when illuminating the copper covered with p-type Cu<sub>2</sub>O may

**Table 6.** Parameters from polarization curves and EIS fitting for 50 nm titanium oxide (galvanostatic) in 0.5 M H<sub>2</sub>SO<sub>4</sub> either saturated with oxygen or nitrogen. Same parameters for 12 nm copper oxide, in borate buffer (pH 9) either naturally aerated or nitrogen purged. The values for the aerated samples are the same as shown in Figure 1 and 2. Illumination: UV—320 nm monochromatic, W—white, D—dark.

Metal	Gas	Illum.	$i_{\text{corr}}$ [ $\mu\text{A cm}^{-2}$ ]	$E_{\text{corr}}$ [mV]	$b_c$ [mV dec. <sup>-2</sup> ]	$b_a$ [mV dec.]	$R_s$ [ $\Omega\text{ cm}^2$ ]	$R_{\text{sc}}$ [ $\Omega\text{ cm}^2$ ]	$Q_{\text{sc}}$ [ $\text{F}^{1/n_{\text{sc}}}\text{ cm}^{-2}$ ]	$n_{\text{sc}}$	$R_{\text{ct}}$ [ $\Omega\text{ cm}^2$ ]	$Q_{\text{dl}}$ [ $\text{F}^{1/n_{\text{dl}}}\text{ cm}^{-2}$ ]	$n_{\text{dl}}$
Ti	O <sub>2</sub> -sat.	D	0.11(2)	222(12)	-121(4)	NA	2.7(1)	1.1(1)E4	1.92(7)E-5	0.90(2)	4(7)E7	5.9(7)E-5	0.90(0)
		UV	0.21(2)	185(8)	-129(1)	557(19)	2.8(1)	1.0(1)E4	2.20(4)E-5	0.89(1)	3.6(5)E5	7.0(9)E-5	0.90(1)
	N <sub>2</sub> -purged	D	0.27(3)	252(7)	-147(18)	396(13)	2.6(1)	5.11(3)E3	4.2(2)E-5	0.83(2)	2.9(5)E5	6.8(8)E-5	0.86(1)
		UV	0.48(3)	225(5)	-160(8)	504(4)	2.5(1)	4.4(3)E3	4.3(4)E-5	0.84(2)	1.3(2)E5	7.7(1)E-5	0.85(1)
Cu	Aerated	D	3.01(8)	-34(1)	-311(68)	132(30)	107(1)	3.2(9)E3	2.5(1)E-5	0.74(1)	4.7(6)E4	1.7(1)E-5	0.52(4)
		W	3.24(8)	-34(1)	-224(18)	100(9)	108(1)	2.5(3)E3	2.6(1)E-5	0.74(1)	3.5(1)E4	1.9(0)E-5	0.52(1)
	N <sub>2</sub> -purged	D	2.1(4)	-62(12)	-289(4)	142(9)	167(3)	1.0(1)E3	2.2(1)E-5	0.80(1)	2.9(0)E4	2.0(1)E-4	0.53(1)
		W	3.1(1)	-68(12)	-217(10)	122(26)	160(9)	1.1(1)E3	4(1)E-5	0.78(1)	2.4(3)E4	3.3(1)E-4	0.52(1)

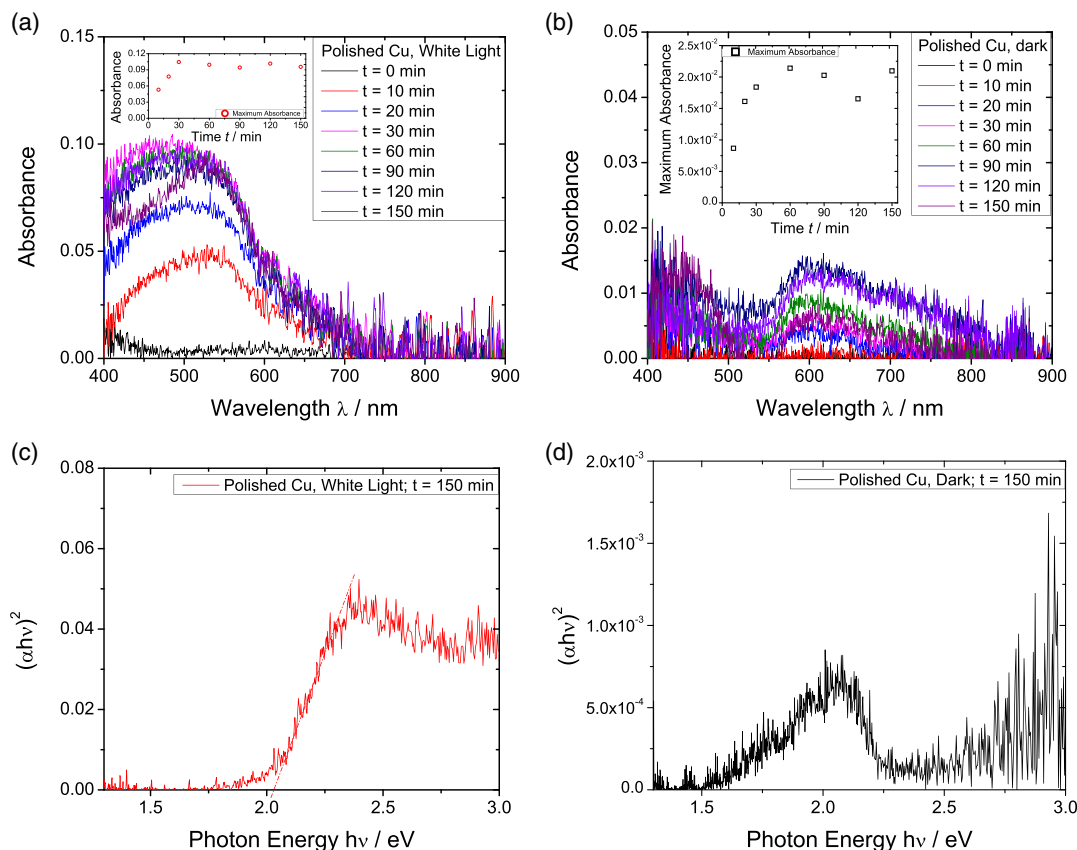


**Figure 11.** In situ reflectance UV-vis spectroscopy of polished copper exposed at open circuit to borate buffer (pH 9) with a) white light illumination for 150 min and b) white light illumination applied only during UV-vis measurements (background: first measurement). Tauc plots of the spectra taken at  $t = 150$  min, c) exposed to white light, d) kept in the dark except for measurements.

therefore be related to an increase of the passive current, and not necessarily directly related to dissolution of the oxide. Illumination causes electron-hole pairs to be generated, which increase the available electrons for the cathodic reaction, and can in that way increase the corrosion current.

No evidence was found here for the photoreduction of  $\text{Cu}_2\text{O}$ , as, for example, reported for electrocatalysts.<sup>[60,61]</sup> The increased dissolution found by ex situ ICP-MS, the increased corrosion current density, and at the same time, the increasing oxide thickness at OCP as evidenced via increasing UV-vis absorbance for polished copper all speak against the formation of metallic copper at least as the dominating process.

The potential dependency of the photocurrent and EIS measurements show that the observed photocorrosion is indeed caused by the semiconductor properties of the oxide. No steady-state photocurrent was observed below the flat band potential for titanium (n-type characteristic) and above the flat band potential for copper (p-type characteristic). Both peak-value and shape of the photocurrent transient change with potential for titanium. The steady-state photocurrent increased with increased overpotential. A wider space charge layer is expected with increased band bending, which occurs at increased potential. A wider space charge layer would facilitate a larger volume where excitation would occur and lead to a photocurrent. Additionally, increased electric field strength across the space charge layer might explain why no decrease in the photocurrent was found after the initial peak and why no cathodic current was measured immediately after illumination was shut off when titanium was

polarized above  $E_{fb}$ . An increased electric field might have prevented back reactions from occurring. For anodized copper similar observations to titanium were made, but in opposite direction. In contrast to titanium, the shape of the phototransient did not change with potential.

For titanium,  $R_{sc}$  increased with increasingly positive potential indicating increased upward band bending. Increased band bending may explain the change in transient shape and increase in the steady-state value of the photocurrent. For copper,  $R_{sc}$  increased with increasingly negative potentials, indicating downward band bending. A schematic band diagram is presented in **Figure 12**. Note that the titanium model is only valid for the potentiostatic anodizing presented in this section. The reason for the model not being valid for galvanostatically anodized titanium is discussed in Section 3.6.

The band bending for anodized titanium polarized close to  $E_{fb}$  (Figure 12a) is in line, for example, with EIS measurements and photocurrent measurements at  $E_{fb}$  (Figure 7a,b): no difference for illuminated and non-illuminated samples was found for the EIS measurements and  $i_{photo} = 0$ . Illuminating even with photon energies above the bandgap did not affect the corrosion process because the electron-hole pairs recombined as there was no space charge layer to separate the charge carriers. Figure 12b shows the situation above  $E_{fb}$  where charge separation is possible:  $|i_{photo}| > 0$ , and a difference between dark and illuminated samples was observed from EIS (Figure 7). Considering the measured anodic photocurrent (Figure 1a), negative photovoltage (Figure 1b), and the n-type properties of the oxide, it is clear that

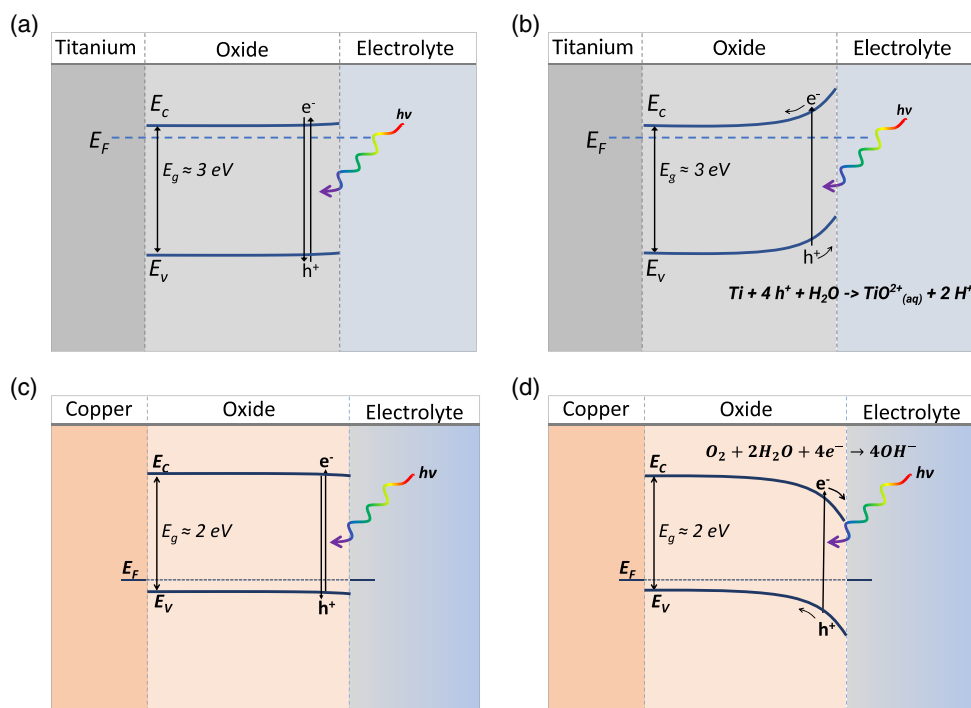


**Figure 12.** Schematics of band bending that causes increased corrosion for anodized titanium and copper when illuminated. a) Titanium polarized to potentials below flat band, b) titanium polarized to potentials above the flat band. c) Copper polarized to potential above the flat band, and d) copper polarized to potential below the flat band.

the holes moved toward the oxide–electrolyte interface. Illumination did then cause the titanium oxide to dissolve through hole annihilation.

When copper was polarized to potentials above  $E_{fb}$ , no photocurrent was found (Figure 8a), opposite of what was found for titanium. This opposite effect is expected and caused by the different semiconductor types. Figure 12c shows the case when the potential is close to  $E_{fb}$ , and recombination occurs. When polarized to potentials below  $E_{fb}$ , a cathodic photocurrent was observed. The band bending schematic explaining the cause of the cathodic photocorrosion is shown in Figure 12d. Since a cathodic photocurrent was found it is postulated that this photocurrent led to increased cathodic reaction rates. In Section 3.5, hydrogen evolution as a reaction without the presence of oxygen is suggested under illumination.

### 3.2. Fluctuations in the Electronic Structure Must Be Present

Fluctuations in the band structure, temporal or spatial, must be present to account for the observed increased corrosion current densities, for the same arguments described previously.<sup>[3]</sup> This work showed cathodic photocurrents for p-type oxide-covered copper, and anodic photocurrents for n-type oxide-covered titanium, and increased corrosion currents. The increased corrosion currents require both an anodic and a cathodic reaction on the same surface; however, the described band bending which enables increased cathodic reactions should at the same time suppress anodic reactions, and vice versa. Lateral heterogeneity (cathodic and anodic reactions at different sites, for example, inside pores and on free oxide surface) or fluctuations in the band edges with distance can encounter for the observed increased corrosion currents.

### 3.3. Heating as an Alternative Explanation

There are two identified ways illumination may affect the corrosion process by heating the oxide surface, i) increased convection by localized heating of electrolyte close to an illuminated surface, and (ii) heating of the oxide and buildup of temperature gradients.

Any significant effect from convection can easily be discarded based on the data presented previously,<sup>[8]</sup> as the temperature increase in electrolyte in the experimental setup used here was at maximum 0.2 °C. Additionally, heating caused by light would not cause the potential-dependent photocurrents shown in Figure 7 and 8, and the monochromatic photocurrent shown in Figure 4b. The transient shape also does not support a heating-based mechanism, as the photocurrents are instantaneous, both when the light is turned on, but for heating purposes more importantly when light is turned off. Discarding any effect from localized heating in the oxide itself is difficult, and a significant increase in corrosion current density was observed when illuminating polished titanium and copper. For titanium, no photocurrent was measured when polished, so here thermal effects in the oxide might play a role. Photocurrents were actually observed for polished copper, but  $\Delta i_{corr}^{(photo)} > i_{photo}$ , so thermal effects inside the oxide layer may also affect copper.

### 3.4. Differences between Potentiostatically and Galvanostatically Anodized Titanium

The photocorrosion mechanism shown earlier for potentiostatically anodized titanium cannot describe the observed photocorrosion of galvanostatically anodized titanium, because  $\Delta i_{corr}^{(photo)} \gg i_{photo}$  (35 times higher), and there were significant differences in Tafel slopes (i.e., shape of the polarization curves) with and without illumination. The different shapes of polarization curves indicate a different reaction mechanism when illuminated with UV light compared to the dark.

A systematic investigation of the differences has not been conducted, however, a hypothesis can be formed. Slowly grown oxides have been reported to be denser and more ordered than quickly grown oxides.<sup>[62,63]</sup> Under the parameters used in this work, galvanostatic anodizing was slower than potentiostatic anodizing. The slower grown titanium oxide also has been reported to exhibit better corrosion resistance. When comparing dark corrosion rates for potentiostatically anodized titanium ( $1.5(2) \mu\text{A cm}^{-2}$ ) to the dark corrosion rates ( $0.16(5) \mu\text{A cm}^{-2}$ ) for the galvanostatically anodized titanium, it is clear that the galvanostatic films offer better corrosion resistance, possible because of more dense and ordered oxide films. In general, processing routes greatly affect the structure and functional properties of  $\text{TiO}_2$ .<sup>[64,65]</sup>

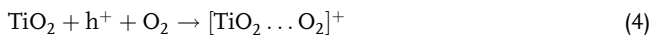
### 3.5. The Role of Oxygen in Photocorrosion

Results presented in Figure 10 show that oxygen concentration affects the corrosion of titanium; in the dark, it has long been known that removing oxygen from sulfuric acid can increase the titanium corrosion rate,<sup>[66]</sup> because oxygen contributes to the passivation. Illumination seemingly prevents this additional passivating contribution from oxygen. One previous explanation of photocorrosion has been that radicals generated by illumination cause increased corrosion rates. Previously, the possibility of UV light to create oxygen radicals has been proposed as a contributor to photocorrosion.<sup>[13,67]</sup> However, to have significant concentrations of radicals generated by photodissociation, illumination is required with photon energies above the energy difference between highest occupied and lowest unoccupied molecular orbital of oxygen, which was not the case in this work. The mechanism of radical formation is thus not directly obvious. Experiments on polished titanium in  $\text{H}_2\text{O}_2$ -containing solution with illumination to generate hydroxyl radicals showed no difference in corrosion rate with or without illumination, indicating that at least hydroxyl radicals do not affect the corrosion of titanium to any significant degree.<sup>[68]</sup> The formation and decomposition of ozone has also been discussed in the frame of photocorrosion of copper, but ozone generation by illumination was not found to have a detectable effect on corrosion rates.<sup>[56]</sup>

The differences between photocorrosion in the absence and presence of oxygen can be seen as indirect evidence for the involvement of radicals in the photocorrosion mechanism, however, no direct evidence for or against photo-produced radicals has been found in this work. Radical intermediates play a role in the cathodic reactions, oxygen reduction, and hydrogen evolution.<sup>[69,70]</sup> These radicals can in principle interact with holes or electrons at the surface, or their rate of formation could be



increased be either the holes or electrons. For the biradical  $O_2$ , an increase in adsorption by interaction with the unpaired hole of an electron-hole pair is also possible



A further reaction of the adsorbed oxygen may explain some of the differences observed in the presence of oxygen.

A photocorrosion mechanism involving production and reaction of radicals is unnecessary to explain the results. In literature work on narrow band semiconductors (CuO,  $MnO_2$ ,  $Fe_2O_3$ , and  $BiVO_4$ ), photoluminescence experiments did not lead to detection of radicals under illumination; this result was explained by the band positions relative to the standard potentials for  $O_2/O_2^-$  or  $OH^-/OH$ , where the bandgap is too narrow to produce these radicals.<sup>[71]</sup> Radical formation through illumination is pH dependent, with higher pH depressing the amount of  $\cdot OH$  produced.<sup>[71]</sup> In this work, copper was exposed to pH 9, and still an effect was seen from illumination. Radicals whose production is depressed at high pH, and which have not been observed for narrow band semiconductors, are therefore unlikely to be the main cause of photocorrosion.

Titanium oxide has a wide enough bandgap to produce hydroxyl radicals.<sup>[71]</sup> However,  $\gamma$  radiation did not increase the corrosion rate of titanium, but rather reduced it due to radiolysis of the electrolyte. The resulting  $H_2O_2$  further passivated the titanium.<sup>[72,73]</sup> Consequently, it is not expected that an increase in corrosion rate would take place in the situation in this work.

The effect of oxygen in the electrolyte and the corresponding effect of illumination indicates that photogenerated holes “weakened” the titanium oxide, and led to higher rates of dissolution. Oxygen has been reported to passivate titanium by oxidizing  $Ti^{III}$  to  $Ti^{IV}$ ,<sup>[47]</sup> creating a more stable oxide that reduces the corrosion rate. Electron-hole pair generation has been shown to weaken the titanium oxide,<sup>[74]</sup> which fits well with results here. Dissolved oxygen stabilizes the titanium oxide, while illumination destabilizes it; the result is that  $\Delta i_{corr}^{(photo)}$  ( $O_2$ -saturated)  $\approx i_{corr}^{(dark)}$  ( $N_2$  purged).

For copper,  $N_2$  purging the electrolyte did not result in an significant difference between the dark and illuminated conditions as it did for titanium; however, there are aspects that are remarkable. Comparing the dark polarization curves in aerated and purged electrolyte gives the effect of oxygen itself. A decrease in  $i_{corr}$  and  $E_{corr}$  was found in oxygen-saturated electrolyte. The decrease in corrosion current density can easily be explained by less oxygen in the electrolyte, and therefore a decrease in the cathodic reaction rate. Oxygen saturation leads to an increase in cathodic current, resulting in an increase in corrosion rate. While the corrosion rate increased more with illumination in the nitrogen-purged electrolyte, the absolute corrosion rate for the illuminated samples in the nitrogen-purged electrolyte was lower than when illuminated in oxygen-saturated electrolyte.

Data from the nuclear waste literature shows that radicals caused by radiolysis can cause increased corrosion in electrolytes without oxygen<sup>[75]</sup>; however, radiolysis is caused by illumination in the MeV range, which is far outside what the light source in this work delivers. When illuminated with sufficiently high photon energies, copper can corrode in oxygen free solutions with

hydrogen evolution as cathodic reaction.<sup>[76]</sup> Without irradiation, copper is immune toward corrosion with hydrogen evolution as the cathodic reaction.<sup>[77]</sup> However, the flow cell, syringe pump, and tubing used for the measurements were not kept in an oxygen-free environment during the experiment. Oxygen may therefore have entered the cell during the measurement, so that residual oxygen may explain any observed corrosion in “nominally oxygen free” solutions.

### 3.6. Photocorrosion in the Frame of the Point Defect Model

“Photo-quenching” of the electric field across a passive layer caused by electron-hole pair separation has been proposed to slow down cation vacancy movement. This quenching has been reported to increase pitting resistance in nickel,<sup>[78]</sup> in copper,<sup>[79]</sup> and for 304/316 stainless steel.<sup>[79]</sup> More recently, the point defect model was also used to explain general corrosion of copper.<sup>[14]</sup>

In the PDM, the outer oxide layer does not contribute to the passive behavior of the metals, it is the inner barrier layer that controls the passive current. The results of illumination on anodized iron<sup>[3]</sup> and potentiostatically anodized titanium fit to this explanation. For anodized iron<sup>[3]</sup> and titanium,  $\Delta i_{corr}^{(photo)}$  was equal to or lower than the measured photocurrent, and ICP-MS (this work) or UV-vis<sup>[3]</sup> measurements confirmed increased dissolution with illumination. The amount of dissolved metal and  $\Delta i_{corr}^{(photo)}$  are on the same order of magnitude, meaning that the light does not affect the corrosion process more than the dissolution of the oxide. Illumination causes an additional dissolution reaction to occur (see Section 3.1). The EIS measurements also indicated that the thicker outer layer did not affect the overall reaction significantly, because only one semicircle is visible (Figure 2).

Another way of thinking about photocorrosion of titanium may be to consider the oxide and metal as two different corroding materials. The metal substrate has a passive current through the inner barrier layer, which is independent on the thicker outer layer. The thicker outer oxide is illuminated and is dissolving due to hole annihilation. The light does not affect the passive current in a significant way, because the light is largely absorbed in the thick outer oxide, which does not affect the passive behavior. The simple semiconductor photoelectrochemical model presented by Wilson et al.<sup>[3]</sup> works very well for the potentiostatically anodized titanium. For galvanostatically anodized titanium, the photoelectrochemical model does not work because the increase in corrosion current density with illumination was one order of magnitude higher than the measured photocurrents. Illumination caused the inner semicircle in the EIS of the galvanostatically anodized titanium to decrease, indicating that the resistance of the outer oxide was reduced. The latest revision of the point defect model<sup>[80]</sup> may be suitable to explain the difference between the galvanostatically and potentiostatically anodized titanium. For valve metals like titanium, the PDM includes the outer oxide when explaining the passive behavior of metals. The outer layer can affect the corrosion rate because of the high resistance of the thick oxide. When the resistance of the outer layer increases, the thickness of the inner barrier layer will be reduced and is even predicted to disappear if the resistance of the outer layer becomes high enough.<sup>[80]</sup>

**Table 7.** Mechanisms of photocorrosion observed in refs. [3,8], and in this study together with experimental characteristics and conditions. In applications, different combinations are possible. n.r.—not relevant.

Mechanism	Photovoltage	Photocurrent	Transient	Surface layer type	$E_{\text{corr}}$ vs $E_{\text{fb}}$	Convection
Heating-induced convection	Positive	–	Slow	n.r.	n.r.	Spontaneous
Hole migration to oxide/solution interface	Negative	Anodic	Instantaneous	n-type	$E_{\text{corr}} > E_{\text{fb}}$	Enforced
Hole migration to metal/oxide interface	Positive	Cathodic	Instantaneous	p-type	$E_{\text{corr}} < E_{\text{fb}}$	Enforced

In the PDM, the steady-state current  $I_{\text{ss}}$  is described as  $I_{\text{ss}} \propto \frac{1}{R_{\text{bl}} + R_{\text{ol}}}$ ,<sup>[59]</sup> where  $R_{\text{bl}}$  and  $R_{\text{ol}}$  are the resistance of the barrier layer and outer layer, respectively. This proportionality shows that increased resistance in the outer layer will decrease the steady-state current. Measurements in this work showed that illumination decreased the resistance in the oxide. The outer oxide might become the dominating resistance, because the thickness of the inner barrier layer may decrease with increased outer oxide resistance. A situation where  $R_{\text{ol}} \gg R_{\text{bl}}$  might occur and the steady-state current is then largely determined by the resistance of the outer oxide. The outer oxide is often many orders of magnitude thicker than the barrier layer,<sup>[59]</sup> especially for anodized samples. Therefore, more light can be absorbed in the outer oxide layer, which is then not available to trigger photoinduced processes in the thin inner barrier layer. It may follow that illumination can affect the corrosion process in a larger degree when the outer oxide is determining the corrosion resistance, because of stronger light absorption. Near a metal surface, a standing wave-like pattern develops, with an intensity minimum at the surface, and the first intensity maximum at a quarter of the wavelength in the respective medium, see, for example, discussion in ref. [17]. For potentiostatically anodized titanium, where the outer oxide does not dominate the impedance of the system, a much smaller effect of light was observed than for the galvanostatically anodized titanium where the passive current might be controlled by the outer oxide.

Illumination might affect the outer oxide in several ways. Possible effects include hole accumulation at the oxide–electrolyte interface increasing the electric field through the outer layer. An increase of the amount of charge carriers in the oxide is also possible. Illumination can possibly also decrease the potential drop between the inner barrier layer and the outer oxide. Temperature gradients in the oxide may also play a role.<sup>[3]</sup> Temperature increase in the oxide may lead to increased ion mobility and would lead to increased passive current. Additionally, increased temperature generally increases reaction rates of thermally activated processes. However, no direct evidence of this was obtained.

#### 4. Conclusions

The characteristics of the different photocorrosion mechanisms observed in our studies are summarized in **Table 7**, where also the important characteristics in terms of easily accessible experimental quantities are given. An interesting immediate question from these results is which situation would arise if, on a system with an n-type oxide,  $E_{\text{corr}} < E_{\text{fb}}$ , or the opposite on a system

with p-type oxide. This question cannot be addressed based on these data.

In this work, on copper and titanium, photoactive oxide layers of 10s of nanometer thickness have been prepared by anodizing. The layers were dominated by cuprite  $\text{Cu}_2\text{O}$  and anatase  $\text{TiO}_2$ , respectively, as crystalline phases. The titanium oxides behaved as n-type semiconductors with a bandgap of 3.0–3.2 eV. The copper oxides behaved as p-type semiconductors with a bandgap of 2.0–2.1 eV. When illuminating the oxide under controlled convection with photon energies higher than the bandgap, photocurrents and photovoltages were measured as expected: the n-type titanium oxides showed these at potentials above the flat band potential, while the p-type copper oxide showed photocurrents and photovoltages below the flat band potential. Under the same conditions, increases in the corrosion rates were also observed. For the anodized samples, observed photocurrents and increase in corrosion currents with illumination were of similar order of magnitude, though the photocurrents were slightly higher; on both systems, few milliamperes per centimeter square in photocorrosion rate were measured. Normalized to the incident power, this increase corresponds to an order of magnitude of  $10 \text{ nA W}^{-1}$ .

For the n-type oxides on titanium, photoelectrochemical experiments and Mott–Schottky analyses are consistent with hole migration to the oxide–electrolyte interface in an oxide layer with upward band bending at the corrosion potential. An exception was the oxide with the largest thickness. The results obtained here are inconsistent with a picture of upward band bending in the n-type semiconducting oxide. Oxide dissolution would thus occur by hole annihilation by cation ejection into the electrolyte. ICP-MS measurements show also that the dissolving fraction of titanium increases with illumination.

For the p-type oxide-covered copper, the results in this work are consistent with downward band bending at the corrosion potential for the p-type copper oxide. Electrons in the conduction band migrate to the oxide/electrolyte interface and increase the cathodic current. Ex situ concentration determination of dissolved species showed that the copper dissolution increased with illumination. At the same time, there was evidence for oxide growth.

Despite illumination with a powerful thermal white light source, the maximum increase in corrosion rate for the nonthermal effect was on the order of  $1 \mu\text{A cm}^{-2}$  for both systems, and can be ignored in applications for structural engineering. The effect on initiation of localized corrosion has not been investigated in this work; presumably, even small effects can play a stronger role to that end.

Polished titanium and copper showed no observable photocurrents, yet the corrosion rate increased when illuminated, even

under controlled convection. Therefore, thermal effects, for example, originating from temperature gradients in the nanometer-thick oxide films are postulated to contribute to photocorrosion. Increased temperature in the oxide can facilitate ionic or defect flux through the barrier layer and thus increase the passive current.

On galvanostatically anodized titanium, the corrosion current density is only 1/10 of that of potentiostatically anodized titanium in the dark, which is a remarkable result. Valve metals are specially considered in the PDM because the outer oxide layer can contribute to corrosion resistance through increased impedance, which may be the case here. EIS showed that illumination reduces this impedance, and in this way, light might significantly affect the corrosion rate of valve metals under the condition that the outer oxide layer contributes to the passivation. An increase in corrosion current of over 40× was found for galvanostatically anodized titanium when illuminating with 320 nm monochromatic light, compared to the dark. This was the biggest increase observed in this work. Even though illumination did in some of the cases for potentiostatically anodized titanium more than double the corrosion currents, the total corrosion current is small,  $\approx 6 \mu\text{m year}^{-1}$  ( $7 \mu\text{A cm}^{-2}$ ). While this corrosion rate is small for use in structural materials, these are appreciable degradation rates in relevant use cases when discussing nanostructures, for example, in catalysts.

## Supporting Information

Supporting Information is available from the Wiley Online Library or from the author.

## Acknowledgements

We thank Sintef Biotechnology and Nanomedicine for the ex situ concentration determination by ICP-MS.

## Conflict of Interest

The authors declare no conflict of interest.

## Author contributions

H.W.: Sample preparation, conduction of most of the photoelectrochemical experiments, data analysis, manuscript writing—original draft. A.V.R.: Sample preparation of galvanostatically anodized titanium. Electrochemical experiments with these samples. K.J.: In situ ICP-MS measurements. J.K.: In situ ICP-MS measurements. A.K.: In situ ICP-MS measurements. S.C.: Supervision of in situ ICP-MS measurements. S.S.: Supervision. A.E.: Supervision, manuscript writing—revision.

## Data Availability Statement

The data that support the findings of this study are openly available in NTNU Open Research Data at <https://doi.org/10.18710/SOTK4W>.

## Keywords

anodic films, passivity, photoanodes, photocathodes, photocathodic protection, photoelectrochemical water splitting, photoelectrochemistry

Received: December 15, 2021

Revised: March 18, 2022

Published online: April 21, 2022

- [1] A. W. Hassel, J. W. Schultze, in *Encyclopedia of Electrochemistry*, (Ed. A. J. Bard, M. Stratmann, G. S. Frankel), vol. 4, Wiley-VCH, Weinheim **2007**, pp. 460–490, Chapter 3.2.
- [2] T. Burleigh, C. Ruhe, J. Forsyth, *Corrosion* **2003**, 59, 774.
- [3] H. Wilson, S. Sunde, A. Erbe, *Corros. Sci.* **2021**, 185, 109426.
- [4] L. Song, X. Ma, Z. Chen, B. Hou, *Corros. Sci.* **2014**, 87, 427.
- [5] P. Qiu, Z. Chen, H. Yang, L. Yang, L. Luo, C. Chen, *Int. J. Electrochem. Sci.* **2016**, 11, 10498.
- [6] A. Benedetti, C. Zanotti, P. Giuliani, M. Faimali, *Corros. Sci.* **2014**, 84, 125.
- [7] A. Benedetti, L. Magagnin, F. Passaretti, E. Chelossi, M. Faimali, G. Montesperelli, *Electrochim. Acta* **2009**, 54, 6472.
- [8] H. Wilson, A. Erbe, *Electrochem. Commun.* **2019**, 106, 106513.
- [9] Y. Liu, J. Zhang, Y. Wei, Z. Wang, *Mater. Chem. Phys.* **2019**, 237, 121855.
- [10] E. Thompson, T. Burleigh, *Corros. Eng. Sci. Technol.* **2007**, 42, 237.
- [11] A. L. Rudd, C. B. Breslin, *J. Electrochem. Soc.* **2000**, 147, 1401.
- [12] A. L. Rudd, C. B. Breslin, *Electrochim. Acta* **2000**, 45, 1571.
- [13] S. Song, Z. Chen, *J. Electrochem. Soc.* **2014**, 161, C288.
- [14] J. Wu, J. Wang, Y. Wu, *Mater. Chem. Phys.* **2020**, 255, 123648.
- [15] L. Song, Z. Chen, *J. Electrochem. Soc.* **2015**, 162, C79.
- [16] F. Di Quarto, F. Di Franco, S. Miraghaei, M. Santamaria, F. La Mantia, *J. Electrochem. Soc.* **2017**, 164, C516.
- [17] A. Erbe, A. Sarfraz, C. Toparli, K. Schwenzfeier, F. Niu *Soft Matter at Aqueous Interfaces*, (Ed. P. R. Lang, Y. Liu), Lect. Notes Phys., Vol. 917, Springer, Cham, Switzerland **2016**, pp. 459–490, Chapter 14.
- [18] S. Chen, D. Huang, P. Xu, W. Xue, L. Lei, M. Cheng, R. Wang, X. Liu, R. Deng, *J. Mater. Chem. A* **2020**, 8, 2286.
- [19] B. Weng, M.-Y. Qi, C. Han, Z.-R. Tang, Y.-J. Xu, *ACS Catal.* **2019**, 9, 4642.
- [20] E. Çepni, H. Öztürk Doğan, *Phys. Status Solidi A* **2020**, 217, 2000323.
- [21] Y.-H. Zhang, M.-M. Liu, J.-L. Chen, S.-M. Fang, P.-P. Zhou, *Dalton Trans.* **2021**, 50, 4091.
- [22] I. V. Bagal, N. R. Chodankar, M. A. Hassan, A. Waseem, M. A. Johar, D.-H. Kim, S.-W. Ryu, *Int. J. Hydrogen Energy* **2019**, 44, 21351.
- [23] C. Y. Toe, J. Scott, R. Amal, Y. H. Ng, *J. Photochem. Photobiol. C* **2019**, 40, 191.
- [24] J. Knöppel, A. Kormányos, B. Mayerhöfer, A. Hofer, M. Bierling, J. Bachmann, S. Thiele, S. Cherevko, *ACS Phys. Chem. Au* **2021**, 1, 6.
- [25] D. Dworschak, C. Brunnhofer, M. Valtiner, *ACS Appl. Mater. Interfaces* **2020**, 12, 51530.
- [26] S. Yaseen, M. B. Tahir, A. G. Wattoo, *Int. J. Energy Res.* **2022**, 46, 634.
- [27] X. Ning, G. Lu, *Nanoscale* **2020**, 12, 1213.
- [28] H. Park, K. Y. Kim, W. Choi, *Chem. Commun.* **2001**, 281.
- [29] V. S. Saji, *J. Electrochem. Soc.* **2020**, 167, 121505.
- [30] Y. Ohko, S. Saitoh, T. Tatsuma, A. Fujishima, *J. Electrochem. Soc.* **2001**, 148, B24.
- [31] Y. Bu, J.-P. Ao, *Green Energy Environ.* **2017**, 2, 331.
- [32] T. Tatsuma, S. Saitoh, Y. Ohko, A. Fujishima, *Chem. Mater.* **2001**, 13, 2838.
- [33] V. Augustyn, P. Simon, B. Dunn, *Energy Environ. Sci.* **2014**, 7, 1597.

- [34] B. Millet, C. Fiaud, C. Hinnen, E. Sutter, *Corros. Sci.* **1995**, 37, 1903.
- [35] E. Sutter, B. Millet, C. Fiaud, D. Lincot, *J. Electroanal. Chem.* **1995**, 386, 101.
- [36] C. Toparli, A. Sarfraz, A. D. Wieck, M. Rohwerder, A. Erbe, *Electrochim. Acta* **2017**, 236, 104.
- [37] F. S. B. Kafi, R. P. Wijesundera, W. Siripala, *Phys. Status Solidi A* **2020**, 217, 2000330.
- [38] N. Fredj, T. Burleigh, *J. Electrochem. Soc.* **2011**, 158, C104.
- [39] J. Knöppel, S. Zhang, F. D. Speck, K. J. Mayrhofer, C. Scheu, S. Cherevko, *Electrochem. Commun.* **2018**, 96, 53.
- [40] K. J. Jenewein, A. Kormányos, J. Knöppel, K. J. J. Mayrhofer, S. Cherevko, *ACS Meas. Sci. Au* **2021**, 1, 74.
- [41] H. Wilson, A. Van Rooij, K. Jenewein, Knöppel, A. Kormányos, S. Cherevko, S. Sunde, A. Erbe, *Replication data for: Photocorrosion of n- and p-type semiconducting oxide covered metals: Case studies of anodized titanium and copper*, NTNU Open Research Data, **2022**, <https://doi.org/10.18710/SOTK4W>.
- [42] J. Gómez-Aguilar, J. Escalante-Martnez, C. Calderón-Ramón, L. Morales-Mendoza, M. Benavidez-Cruz, M. Gonzalez-Lee, *Adv. Math. Phys.* **2016**, 2016, 1.
- [43] A. R. C. Bredar, A. L. Chown, A. R. Burton, B. H. Farnum, *ACS Appl. Energy Mater.* **2020**, 3, 66.
- [44] F. Fabregat-Santiago, G. Garcia-Belmonte, J. Bisquert, A. Zaban, P. Salvador, *J. Phys. Chem. B* **2002**, 106, 334.
- [45] T. Lopes, L. Andrade, F. Le Formal, M. Gratzel, K. Sivula, A. Mendes, *Phys. Chem. Chem. Phys.* **2014**, 16, 16515.
- [46] B. Klahr, S. Gimenez, F. Fabregat-Santiago, J. Bisquert, T. W. Hamann, *J. Am. Chem. Soc.* **2012**, 134, 16693.
- [47] J. Vaughan, A. Alfantazi, *J. Electrochem. Soc.* **2006**, 153, B6.
- [48] A. Folger, P. Ebbinghaus, A. Erbe, C. Scheu, *ACS Appl. Mater. Interfaces* **2017**, 9, 13471.
- [49] A. Raghav, A. Tri Hanindriyo, K. Utimula, M. Abbasnejad, R. Maezono, E. Panda, *Comput. Mater. Sci.* **2020**, 184, 109925.
- [50] M. Arrigoni, G. K. H. Madsen, *J. Chem. Phys.* **2020**, 152, 044110.
- [51] Y. Shi, H. Sun, M. C. Nguyen, C. Wang, K. Ho, W. A. Saidi, J. Zhao, *Nanoscale* **2017**, 9, 11553.
- [52] S. Selçuk, A. Selloni, *J. Chem. Phys.* **2014**, 141, 084705.
- [53] E. V. Lavrov, I. Chaplygin, F. Herklotz, V. V. Melnikov, *Phys. Status Solidi B* **2021**, 258, 2100171.
- [54] C. Toparli, A. Sarfraz, A. Erbe, *Phys. Chem. Chem. Phys.* **2015**, 17, 31670.
- [55] C. Toparli, S. W. Hieke, A. Altin, O. Kasian, C. Scheu, A. Erbe, *J. Electrochem. Soc.* **2017**, 164, H734.
- [56] H. Lin, G. Frankel, *Corros. Eng. Sci. Technol.* **2013**, 48, 461.
- [57] H. Li, Z. Chen, X. Liu, J. Hou, M. Sun, R. Zeng, *J. Electrochem. Soc.* **2018**, 165, C608.
- [58] R. Memming, *Semiconductor Electrochemistry*, 2nd ed., Wiley-VCH, Weinheim, Germany, **2015**.
- [59] D. D. Macdonald, *Electrochim. Acta* **2011**, 56, 1761.
- [60] F. D. Speck, S. Cherevko, *Electrochem. Commun.* **2020**, 115, 106739.
- [61] C. Y. Toe, Z. Zheng, H. Wu, J. Scott, R. Amal, Y. H. Ng, *Angew. Chem. Int. Ed.* **2018**, 57, 13613.
- [62] T. Shibata, Y.-C. Zhu, *Corros. Sci.* **1995**, 37, 253.
- [63] N. K. Kuromoto, R. A. Simão, G. A. Soares, *Mater. Charact.* **2007**, 58, 114.
- [64] W. Raza, I. Hwang, N. Denisov, P. Schmuki, *Phys. Status Solidi A* **2021**, 218, 2100040.
- [65] M. El Achhab, A. Erbe, G. Koschek, R. Hamouich, K. Schierbaum, *Appl. Phys. A* **2014**, 116, 2039.
- [66] *Imperial Metal Industries (Kynoch) Limited, Corrosion resistance of titanium*, Birmingham, Reading, Massachusetts, **1969**.
- [67] H. Riazi, I. Danaee, M. Peykari, *Met. Mater. Int.* **2013**, 19, 217.
- [68] K. Nakamura, Y. Yamada, Y. Takada, T. Mokudai, H. Ikai, R. Inagaki, T. Kanno, K. Sasaki, M. Kohno, Y. Niwano, *Dent. Mater. J.* **2012**, 31, 941.
- [69] S. Nayak, P. U. Biedermann, M. Stratmann, A. Erbe, *Phys. Chem. Chem. Phys.* **2013**, 15, 5771.
- [70] S. Nayak, P. U. Biedermann, M. Stratmann, A. Erbe, *Electrochim. Acta* **2013**, 106, 472.
- [71] Q. Xiang, J. Yu, P. K. Wong, *J. Colloid Interface Sci.* **2011**, 357, 163.
- [72] Y. Kim, R. Oriani, *Corrosion* **1987**, 43, 92.
- [73] Y. Kim, R. Oriani, *Corrosion* **1987**, 43, 85.
- [74] M. Mikula, M. Ceppan, J. Panák, *Corrosion* **1995**, 51, 206.
- [75] Å. Björkbacka, S. Hosseinpour, M. Johnson, C. Leygraf, M. Jonsson, *Radiat. Phys. Chem.* **2013**, 92, 80.
- [76] R. Latanision, G. K. Chuah, D. D. Macdonald, D. Shoesmith, *Mechanism of copper corrosion in aqueous environments*, Technical Report 2009:4e, Swedish National Council for Nuclear Waste, **2009**, [http://www.mkg.se/uploads/Swedish\\_National\\_Council\\_for\\_Nuclear\\_Waste\\_Report\\_2009-4e\\_Mechanisms\\_of\\_Copper\\_Corrosion\\_in\\_Aqueous\\_Environments.pdf](http://www.mkg.se/uploads/Swedish_National_Council_for_Nuclear_Waste_Report_2009-4e_Mechanisms_of_Copper_Corrosion_in_Aqueous_Environments.pdf).
- [77] N. de Zoubov, C. Vanleugenhaghe, M. Pourbaix, *Atlas of electrochemical equilibria in aqueous solutions*, (Ed. M. Pourbaix), National Association of Corrosion Engineers/Centre Belge d'Etude de la Corrosion CEBELCOR, Houston/Bruxelles, USA/Belgium, **1974**, pp. 384–392, Chapter 14.1.
- [78] S. Lenhart, M. Urquidi-Macdonald, D. Macdonald, *Electrochim. Acta* **1987**, 32, 1739.
- [79] C. B. Breslin, D. D. Macdonald, *Electrochim. Acta* **1998**, 44, 643.
- [80] D. Macdonald, G. Englehardt, *ECS Trans.* **2010**, 28, 123.
- [81] L. Song, Z. Chen, *Corros. Sci.* **2014**, 86, 318.
- [82] X. Qiu, J. Li, Z. Liu, *Int. J. Electrochem. Sci.* **2019**, 14, 3236.
- [83] P. Qiu, H. F. Yang, L. J. Yang, Z. S. Chen, L. J. Lv, Y. Song, C. F. Chen, *Mater. Corros.* **2017**, 68, 1004.
- [84] D. F. Heaney, D. D. Macdonald, *J. Electrochem. Soc.* **1999**, 146, 1773.
- [85] P. Schmuki, H. Böhni, *Electrochim. Acta* **1995**, 40, 775.
- [86] D. Macdonald, E. Sikora, M. Balmes, R. Alkire, *Corros. Sci.* **1996**, 38, 97.
- [87] C. B. Breslin, D. D. Macdonald, J. Sikora, E. Sikora, *Electrochim. Acta* **1997**, 42, 127.
- [88] C. B. Breslin, D. D. Macdonald, E. Sikora, J. Sikora, *Electrochim. Acta* **1997**, 42, 137.
- [89] S. Moussa, M. Hocking, *Corros. Sci.* **2001**, 43, 2037.
- [90] H. Luo, X. Li, C. Dong, K. Xiao, X. Cheng, *J. Phys. Chem. Solids* **2013**, 74, 691.
- [91] D. D. Macdonald, D. F. Heaney, *Corros. Sci.* **2000**, 42, 1779.
- [92] S. Qian, Y. Liu, L. Yin, X. Wu, J. Li, J. Wang, F. Lyu, Y. Jiang, *J. Electrochem. Soc.* **2020**, 167, 021506.
- [93] X. Sun, Z. Chen, J. Li, J. Hou, L. Xu, *Int. J. Electrochem. Sci.* **2018**, 13, 8150.
- [94] J. Wu, J. Wang, *Corros. Sci.* **2019**, 154, 144.
- [95] H. Lin, G. Frankel, *J. Electrochem. Soc.* **2013**, 160, C336.
- [96] T. Ohtsuka, T. Otsuki, *J. Electroanal. Chem.* **1999**, 473, 272.
- [97] K. Fushimi, K. Kurauchi, H. Ikeyama, Y. Kitagawa, T. Nakanishi, Y. Hasegawa, M. Ueda, T. Ohtsuka, *J. Solid State Electrochem.* **2015**, 19, 3579.
- [98] K. Fushimi, K. Kurauchi, T. Nakanishi, Y. Hasegawa, M. Ueda, T. Ohtsuka, *Corros. Sci. Technol.* **2016**, 15, 265.
- [99] A. Michaelis, S. Kudelka, J. Schultze, *Electrochim. Acta* **1998**, 43, 119.
- [100] A. Michaelis, S. Kudelka, J. Schultze, *Corros. Rev.* **2000**, 18, 395.
- [101] Y. Hisano, K. Takasawa, N. Hara, K. Sugimoto, *Zairyo-to-Kankyo* **2003**, 52, 199.

- [102] Z. Chen, D. Liang, G. Ma, G. Frankel, H. Allen, R. Kelly, *Corros. Eng. Sci. Technol.* **2010**, 45, 169.
- [103] D. Liang, H. Allen, G. Frankel, Z. Chen, R. Kelly, Y. Wu, B. Wyslouzil, *J. Electrochem. Soc.* **2010**, 157, C146.
- [104] R. Wiesinger, M. Schreiner, C. Kleber, *Appl. Surf. Sci.* **2010**, 256, 2735.
- [105] E. Juzeliunas, P. Kalinauskas, A. Stankeviciute, A. Sudavivius, A. Survila, *Corrosion* **1995**, 51, 672.
- [106] E. Juzeliu, P. Kalinauskas, P. Miečinskas, *J. Electrochem. Soc.* **1996**, 143, 1525.
- [107] P. Kalinauskas, I. Valsiunas, M. Samulevicien, E. Juzeliunas, *Corros. Sci.* **2001**, 43, 2083.